Optogenetic activation of dorsal raphe serotonin neurons induces brain-wide activation, including reward-related circuits

Hiro Taiyo Hamada[1,3,*], Yoshifumi Abe[2], Norio Takata[2], Masakazu Taira[1], Kenji F. Tanaka[2], Kenji Doya[1,*]

[1] Neural Computation Unit, Okinawa Institute of Science and Technology Graduate University, Okinawa, Japan
[2] Department of Neuropsychiatry, Keio University School of Medicine, Tokyo, Japan
[3] Research & Development Department, Araya Inc., Tokyo, Japan
* Correspondence to hamada_h@araya.org, doya@oist.jp

Abstract

Serotonin is a neuromodulator that affects multiple behavioral and cognitive functions. Nonetheless, how serotonin causes such a variety of effects through brain-wide projections and various receptors remains unclear. Here we measured the brain-wide response to optogenetic stimulation of serotonin neurons in the dorsal raphe nucleus (DRN) with functional MRI using an 11.7T scanner with a cryoprobe. Transient activation of DRN serotonin neurons caused brain-wide activation, including reward-related brain areas. The same stimulation under anesthesia with isoflurane decreased activation of reward-related areas and the hippocampal complex. These brain-wide response patterns can be explained by DRN serotonergic projection topography and serotonin receptor expression profiles, with enhanced weights on 5-HT1 receptors. Together, these results provide foundational understanding of the primarily facilitatory effect on brain areas by the DR serotonergic system, which is consistent with recent discoveries of its roles in adaptive behaviors.

Introduction

Serotonin, 5-hydroxytryptamine (5-HT), serves crucial behavioral and cognitive functions, including awake-sleep cycle, mood, reward and punishment predictions [5, 32], patience [37, 39], and learning [19]. Serotonin is also a major target of medications for psychiatric disorders, notably major depression, by selective serotonin re-uptake inhibitors (SSRIs). The dorsal raphe nucleus (DRN) is a major source of serotonergic projections to brain-wide targets, including the frontal cortex, the basal ganglia, the ventral tegmental area (VTA), and other mid-brain regions [50]. The DRN contains glutamatergic, GABAergic, and dopaminergic neurons, in addition to serotonergic neurons [12]. Optogenetic manipulation of serotonin neuron activities has revealed their roles in reward [25-26] , patience [37, 39], anxiety [30, 43], and learning [19, 44]. Nonetheless, how brain-wide serotonergic projections cause such effects and by which target areas and receptors, remain poorly understood [38, 63].

In order to clarify the global picture of serotonergic control of brain activities, we performed optogenetic functional MRI experiments using Tph2-ChR2(C128S) transgenic mice and an 11.7T MRI scanner with a cryoprobe for high S/N measurement. A previous optogenetic fMRI experiment activated DRN serotonin neurons using the Pet1 promoter under anesthesia and showed widespread suppression of cortical activities [16]. We introduced an acclimation protocol to allow stable fMRI recording from awake mice [1, 66] and found that DRN serotonin activation in an awake state induced a brain-wide activity increase both in the cortical and subcortical areas, including reward-related circuits. In contrast, under anesthesia with isoflurane, DRN serotonin activation decreased activities in those areas, consistent with a previous study [16].

We further found that regional BOLD responses can be approximated by a linear model with projection densities of DRN serotonin neurons and expression profiles of different types of serotonin receptors, with negative coefficients for 5-HT1 receptors and positive coefficients for 5-HT2 receptors. These results suggest that serotonergic neurons activate brain-wide regions, including reward-related circuits, and they demand reconsideration of implications of results under anesthesia.

Results

In order to clarify effects of brain-wide serotonergic projections, we employed optogenetic fMRI combining optogenetic stimulation of serotonergic neurons in the dorsal raphe nucleus (DRN) and measurements of whole-brain activities by functional MRI. We used Tph2-ChR2(C128S) transgenic mice [43, 57] which express step-type channel rhodopsin selectively in serotonin neurons [39, 43]. We used an 11.7T MRI scanner (Bruker BioSpec 117/11) with a cryoprobe for high S/N recording of BOLD signals from the whole brain, except the olfactory bulb and the posterior cerebellum.

Prior to experiments, the transgenic and wild-type (WT) groups (Transgenic group: n = 8; Wild-type: n = 6) underwent surgery to attach a plastic fixation bar and implant an optical cannula in the DRN. Acclimation training in a mock chamber followed (Figure 1. See Methods for details). After fMRI experiments, animals were tested in a reward

waiting task [37, 39] to confirm the effectiveness of optogenetic stimulation (Supplementary Figure S1).

DRN Serotonin activation induces a brain-wide increase in BOLD signals

We measured BOLD responses under optogenetic stimulation of DRN serotonin neurons in an ON/OFF block design protocol (Figure 1e). Photo-stimulation increased BOLD signals in the DRN (Figure 1f), with a tendency for reduced response after repeated stimulation. On average, over five stimulations, blue light stimulation induced a significantly higher BOLD response than did yellow light stimulation ($p < 0.05$, correction of multiple comparisons with the false discovery rate (FDR), see 'General Linear Model (GLM) for BOLD signals' in Methods; Figure 1g and Supplementary Figure S5).

A group analysis with a general linear model (GLM) of photo-activated BOLD responses between blue and yellow stimulation from the transgenic group($n = 8$) revealed a brain-wide increase in BOLD responses, significantly in the frontal cortex, the caudate putamen (CPu), the temporal cortical regions, the thalamic complex, and the VTA ($p < 0.05$, cluster-wise correction controlling family wise error (FWE) with probabilistic threshold-free cluster enhancement (pTFCE); Figure 2a). Trial-wise BOLD responses also showed consistent brain-wide activation by blue, but not yellow stimulation ($p < 0.05$, uncorrected, Supplementary Figure S2a-b).

We next selected 28 regions of interest (ROIs) from the cortex and subcortical areas that are involved in reward and punishment, according to the Allen mouse brain atlas (Table 1, see Regions of interest in Methods). For the reward system, we selected components of basal ganglia such as caudate putamen (CPu), nucleus accumbens (NAc), and globus pallidus (GP) [54]. For the punishment system, the bed nucleus of the stria terminalis (BST) [13], the hippocampus [20], and the lateral habenula (LHb) [59] were selected. Then, we extracted regional average beta values (regression coefficients) from the GLM. Comparison of regional beta values between blue and yellow stimulation from the transgenic group revealed that the BOLD response was significantly higher in the blue illumination session in 12 of 14 cortical regions, including the OFC, mPFC and ACC, and 12 of 14 subcortical regions, including the CPu, NAc, GP, VTA, LHb, and DRN (Figure 2b) although no statistical differences were found in the WT group (Supplementary Figure S4). Moreover, there was no significantly higher BOLD response in vRSC, V1, DG, or CA1.

The week after session 1, we performed another session under the same stimulation parameters as in session 1. Patterns of BOLD responses were similar to those in session 1(transgenic: $n = 7$, WT: $n = 6$, Supplementary Figure S3). Pearson's correlation of the beta values in sessions 1 and 2 was $r = 0.875$, which was statistically significant ($p < 1e-8$; Supplementary Figure S7.a). We further checked regional differences of responses in peak amplitude and peak timing by extracting regional BOLD signals (Supplementary Figure S5-9). Peak amplitude and peak timing of BOLD responses varied across the 28 ROIs (Supplementary Figure S8.c-d), with the largest responses in the VTA, SNr, and FP. Both amplitude and timing of BOLD responses in sessions 1 and 2 were significantly correlated for blue light stimulation (amplitude: $r = 0.886$, $p < 1e-8$;

timing: $r = 0.679$, $p < 0.005$), but not for yellow stimulation (amplitude: $r = -0.06$, $p = 0.766$; $r = 0.037$, $p = 0.855$; Supplementary Figure S8.a, b). These results indicate that our photo-stimulation of DRN induced consistent activation of DRN serotonergic neurons, which caused distinct spatial and temporal responses in multiple cortical and sub-cortical regions.

DRN Serotonin activation induces a brain-wide negative response in BOLD signals under anesthesia

Contrary to our above results, a previous optogenetic fMRI study reported that DR serotonin activation evoked negative cortical cerebral blood volume (CBV) responses, an enhanced proxy of BOLD signals, from the entire cortical region under anesthesia [16]. There are two critical differences between that study and this one: optogenetic probes and anesthesia. The previous study used the ePET-Cre mouse line and AAV harboring Cre-dependent ChR2 and applied 20-Hz photostimulation. On the other hand, the current study used Tph2-ChR2(C128S) transgenic mice, which express step-type opsin, to allow continuous activation by a pulse of blue light (1.0 s, 473 nm) at the beginning and yellow light (1.0 s, 593 nm) at the end (Figure 1e). Another difference is that the previous study employed isoflurane, a general gas anesthetic with a muscle relaxant, while our experiment employed no anesthetics.

In order to test the possibility that the difference is due to anesthesia, we compared BOLD responses to DRN serotonin stimulation between anesthetized and awake states in the same animals. We performed the same ON/OFF stimulation protocol under anesthesia with 1% isoflurane with the same groups (Transgenic: $n = 7$, WT: $n = 5$, Figure 3a). We also performed another ON/OFF stimulation session the next day in an awake state in order to eliminate possible confounding by diminished responses after repetitive photo-stimulation (Figure 3b).

Under anesthesia, we observed mostly negative BOLD responses from the entire cortical region, while BOLD signals in the DRN remained positive (statistical $t > 1$, uncorrected; Figure 3a & Supplementary S10a). On the other hand, session 4 under an awake state replicated positive BOLD signals from mid-line cortical regions and DRN (statistical $t > 1$, uncorrected; Figure 3b & Supplementary Figure S10b). We then contrasted regional beta values in anesthetized and awake states (Figure 3c). In the anesthetized state, multiple regions, such as ACC, dRSC, vRSC, DG and CA1 showed negative beta values, significantly different from those in the awake state ($p < 0.05$, correction of multiple comparisons with FDR). We further found a statistically significant difference in peaks of % BOLDs of these regions between anesthetized and awake states ($p < 0.05$, Figure 3d; Supplementary Figure S11). Our results support the hypothesis that general anesthesia induced negative BOLD responses by DR serotonin photo-activation.

Brain-wide BOLD responses are explained by serotonin projection density and receptor expression profiles

Our results revealed a brain-wide profile of evoked BOLD signals by DR serotonin activation (Figure 2a). One plausible mechanism underlying such a spatial profile is the density of the serotonergic projection pattern from the DRN. In order to test such a

possibility, we checked the correlation between intensity of projections of DRN serotonin neurons and peak levels of BOLD responses. We extracted serotonin-specific structural projection density from DRN from the Allen Brain Atlas (Figure 4a).

Serotonin projection density was statistically correlated with beta values under blue stimulation ($r = 0.462$, $p < 0.05$, FDR corrected) but not under yellow stimulation ($r = 0.132$, $p = 0.529$; Figure 4b). We also found that projection density was significantly correlated with photo-stimulated BOLD responses in awake and anesthetized states (Anesthetized (Session3): $r = 0.546$, $p < 0.05$; Awake (Session4): $r = 0.758$, $p < 0.001$, FDR corrected; Figure 4c).

We further investigated whether photo-stimulated BOLD responses are associated with serotonin synaptic receptors. Gene expression maps for 5-HT1A, 5-HT1B, 5-HT1F, 5-HT2A, and 5-HT2C receptors were obtained from the database of the Allen Brain Atlas (Supplementary Figure S12&S13). We then constructed a multiple linear regression model (MLRM; Figure 5a) composed of one dependent variable of the BOLD response and six independent variables of the projection density and five gene expression patterns (5-HT1a, 5-HT1b, 5-HT1f, 5-HT2a, and 5-HT2c receptors) after normalization. The model reproduced the BOLD response with $R^2=0.66$ ($p < 0.01$, Table 2). We also checked the consistency of the model using BOLD responses in different sessions. Using the fit beta values with session 1, we found a significant correlation with the beta value in session 4 (Awake: $r = 0.615$, $p < 0.01$, FDR corrected, Figure 5b), but not in session 3 (Anesthetized (Session3): $r = 0.365$, $p = 0.079$, FDR corrected; Figure 5c).

We investigated the contribution of each receptor by the estimated regression coefficients in anesthetized and awake states (Figure 5d, Table 3, and Supplementary Table 3). For each subject, we estimated regression coefficients from each session. In the awake state (Session 1,2, and 4), gene expression of 5-HT1 receptors (5-HT1a, 5-HT1b, and 5-HT1f) showed average negative coefficients, indicating negative contributions to BOLD responses. On the other hand, gene expression of 5-HT2 receptors showed average positive coefficients, indicating positive contributions to BOLD responses. We also checked whether expression of each receptor type differed between awake and anesthetized states with one-way analysis of variance (ANOVA). The results revealed that in the anesthetized state (Session 3), weights for 5-HT1f and 5-HT2c receptors were significantly different ($p < 0.05$, Bonferroni corrected, Table 3).

These results suggest that photo-activated BOLD responses reflect projection density of serotonin neurons and serotonin receptor expression profiles and that general anesthesia affects responses of 5-HT1 and 5-HT2 receptors differently to induce altered BOLD responses.

Discussion

Our opto-fMRI investigation of the DRN serotonergic modulations of brain-wide dynamics brought three major discoveries. First, DRN serotonergic activation causes brain-wide positive BOLD responses in an awake state. Second, DRN serotonergic activation under general anesthesia causes brain-wide negative BOLD responses. Third,

the whole-brain profile of DRN serotonin-activated BOLD signals is associated with the density of DRN serotonergic projection and the expression profiles of 5-HT receptors, with opposite weights for 5-HT1 and 5-HT2 receptors.

The present result demonstrating brain-wide activation by DRN serotonergic activation provides a means of interpreting recording and manipulation studies in humans and animals [10, 19, 27, 36-39, 53, 58]. Previous studies have demonstrated serotonin's involvement in motivation and reward-related learning[5, 36] through modulation of the ACC and ventromedial PFC on learning signals [53], CPu on short/long-term prediction of rewards [58], and mPFC and OFC on waiting for delayed rewards [38]. Our opto-fMRI results support those studies, as those areas were consistently activated by DRN serotonin stimulation. In addition, average amplitudes of BOLD responses and peak timing are region-dependent. This finding implies that serotonin-activated BOLD responses are coupled with different regional distributions of receptor densities and serotonin projection, but not with the distance of the activation site. In spite of indirect evidence, our linear approximation of serotonin-activated BOLD responses support such a possibility. A subpopulation of DR serotonin projections to the cortex is also expressed with the vesicular glutamate transporter Vglut3 (Slc17a8). Co-release of glutamate has recently been reported [49-50]. Our results may reflect the influence of serotonin as well as glutamate co-release on downstream circuitry.

Serotonergic modulation in short-term windows using optogenetics can avoid limitations of long-term windows, such as pharmacological manipulation [3, 52] and chemogenetic manipulation with DREADD (designed receptors exclusively activated by designed drugs) [15]. Multiple pharmacological studies have applied SSRIs to manipulate the serotonin system. Systemic SSRI administration causes brain-wide inhibitory modulation [3, 52]. However, the influence of SSRI administration on brain activity can be confounded by the administration period due to receptor sensitivity [11, 22, 52].

A previous study stimulated the serotonin system with specifically designed drugs under fMRI [15] and revealed brain-wide positive responses in the somatosensory cortex and subcortical regions, including the hippocampus, the hypothalamus, and the cerebellum. That study did not reveal BOLD responses of mid-line cortical regions, such as the OFC, mPFC and ACC. A possible explanation for the difference between their results and ours is that BOLD responses cause different time scales, depending on receptor types. Our optogenetic fMRI approach revealed an influence on motivation-related regions at different timings in a transient time window (Supplementary Figure S5, S6 and S8). Further studies using different methodologies, including optogenetics and chemogenetics, will uncover neural mechanisms underlying different time scales of serotonin modulation.

The mechanism underlying different serotonin modulation between awake and anesthetized states remains unknown. One possible mechanism is a reduction of glutamate transmission via serotonin in target regions [60]. Previous studies revealed that isoflurane suppresses neural activity via inhibition of glutamatergic transmission [60, 62]. We found that isoflurane reduced photo-stimulated BOLD signals where they

were potentiated in an awake state. Our results also showed that some regions show potentiated negative BOLD responses. In addition to reduced glutamatergic transmission, isoflurane also enhances sensitivity of GABA neurons [6, 64]. Such elevated responses of GABA neurons and reduced responses of glutamatergic neurons may result in diminished positive BOLD signals and potentiated negative BOLD signals. It is also interesting to ask whether different anesthetics like NMDA antagonists induce different effects on receptor responses while neuron-specific distributions of serotonin receptors are unclear. Serotonin receptors in the prefrontal cortex are differentially distributed [47]. 5-HT1A and 2A receptors are enriched on glutamatergic pyramidal neurons in the PFC [2] . Meanwhile, 5-HT3A receptors are located on GABAergic interneurons [46]. Since different anesthetics influence different neuron types in various ways, reactivity of serotonin receptors may induce different responses. In addition, anesthetics may change effects of serotonin receptors. Some studies showed that isoflurane changes binding affinities of 5-HT_{2B} receptors [33] in vitro and 5-HT_{1A} receptors [65] in vivo. Anesthetics can influence ligand binding to specific subtypes of serotonin receptors.

Furthermore, our results showed negative BOLD response in dorsal hippocampus under anesthesia despite no projections to hippocampus from the DRN. One potential cause is indirect influence by downstream circuitry of DR serotonin neurons. For example, DR serotonin neurons have dense projections to the PFC, which interacts with the hippocampus [9, 29]. Reduction of the BOLD response in the hippocampus under anesthesia can be indirectly caused by activation of DR serotonergic neurons through their downstream circuitry, although the influence is not observable in awake states. The brain-wide response by activation of DR serotonin neurons under anesthesia may have implications for sleep state. Similarity of brain states between general anesthesia and non-rapid-eye-movement (NREM) sleep is implicated [45]. Previous studies also revealed that DR serotonin neurons mediate the sleep/wake cycle [23, 55]. Optogenetic activation of DR serotonin neurons prolonged wakefulness and decreased NREM sleep while their inactivation prevented arousal from CO_2-induced sleep [55]. Similarly, optogenetic and chemogenetic activation induced arousal from isoflurane [23]. The negative response under anesthesia may reflect a brain response associated with arousal. Future studies are needed to clarify the neural mechanism underlying BOLD signals under anesthesia.

We have also demonstrated that different types of 5-HT gene expression are associated with photo-activated BOLD responses. Distinctive contributions of serotonin receptor types influence neural activities mostly at metabotropic receptors [35]. 5-HT1 receptors are inhibitory metabotropic receptors that suppress neural activity by modulating the cellular signal cascade, whereas 5-HT2 receptors are excitatory metabotropic receptors that activate neural activity [42, 48]. Our MLRM analysis revealed that regression coefficients of gene expression of 5-HT1 receptors and 5-HT2 receptors are negative and positive, respectively. The correspondence between functions of receptor types and signs of coefficients implies that BOLD responses by DRN serotonin photo-activation can be influenced by different receptor distributions. Localization of 5-HT receptors is subtype-dependent. 5-HT_{1A} and 5-HT_{1B} receptors are pre-synaptically expressed either on somato-dendrites or within axon terminals of DR serotonin neurons [4, 51], whereas

5-HT_{2A} and 5-HT_{2C} receptors are predominantly expressed on postsynaptic neurons [7, 14]. However, whether 5-HT_{1F} receptors are pre- or post-synaptically expressed is unclear, although they are enriched in cortical layers (layer IV and V) and the caudate putamen [28]. Nonetheless, specifically how 5-HT receptors react to serotonin transmission under general anesthetics is unclear. It is also plausible that general anesthetics change binding affinity of 5-HT receptors [33, 65]. As another potential mechanism, serotonin transmission can be influenced by general anesthetics. Some studies revealed that isoflurane lessens spontaneous serotonin levels and spontaneous firing [31, 61]. These changes of serotonin transmission and receptor binding affinity may influence responses of 5-HT receptors under anesthesia.

The substantial reduction of magnitude of brain-wide responses between the first, second, and third sessions is noteworthy, despite consistent activation patterns. Repeated optogenetic stimulation of DR serotonin neurons and repeated stress potentially account for this reduction. Persistent changes in spontaneous behaviors by repeated optogenetic activation of DR serotonin neurons have been reported [8]. Serotonin is an inducing factor of synaptic plasticity, and repeated stimulation may cause plasticity changes. In addition, repeated restraint stress also may change responses to optogenetic stimulation of DR serotonin neurons, although the habituation protocol to awake fMRI is introduced to prevent restraint stress. Restraint stress increases serotonin release in the amygdala [40]. Molecular and neuronal mechanisms underlying such diminitions are needed to understand long-term effects of serotonin stimulation.

While our results replicated negative cortical responses under anesthesia [16], there are several important differences in methodology and results between previous studies and this one. First, one previous study utilized cerebral blood volume (CBV) signals with a contrast agent to enhance influence of serotonin modulation, although the current study employed BOLD signals. Although CBV signals are an enhanced proxy of BOLD signals, the methodological difference in imaging may show different responses from various brain regions. Second, we employed a transgenic group targeting the tryptophan hydroxylase 2(Tph2) promoter [43, 57] although the previous study employed the ePET-Cre line, targeting transcription factor Pet1 [16]. While expression of ChR2 by Tph2 is selective for serotonergic neurons [41], Pet1 promoters are also expressed in non-serotonergic neurons [26, 34]. While CA1 and DG were significantly deactivated by serotonin photo-activation in our study, responses in temporal regions were not found in the previous study [16]. Additionally, our results reveal an association between 5HT projection density and BOLD responses, but the previous study did not find this association. One critical methodological difference is that we employed different ROIs from those of the previous study. In the current study, 28 ROIs from the Allen brain atlas, included other sources of serotonin and dopamine, the MRN and VTA. In contrast, the previous study used 38 ROIs from the Australian Mouse Brain Mapping Consortium (AMBMC, https://www.imaging.org.au/AMBMC) with multiple ROI hippocampal formations and midbrain regions. The ROI difference may yield different results in the association between structural connectivity and responses to optogenetic serotonin activation. Further research is required to dissect differences between the two sets of experimental results.

In conclusion, we reported brain-wide responses of DRN serotonin activation via opto-fMRI for the first time in awake animals. We found serotonergic modulation of widespread cortical and sub-cortical targets at different timing as a key controller of brain-wide information transmission. We also showed different modulation by the serotonin system in awake and anesthetized states. We further showed that serotonergic structural projections and gene expression profiles of 5-HT receptors are associated with BOLD responses. Further research is required to understand complex serotonin modulation of brain-wide dynamics, given its neural and molecular mechanisms, such as interactions with neural populations and receptors. Our findings reveal a new physiological basis for understanding serotonergic control of brain-wide dynamics and functions.

Materials and Methods

All experimental procedures were performed under protocols approved by the Okinawa Institute of Science and Technology Experimental Animal Committee.

Animals

Serotonin neuron-specific channelrhodopsin 2 variant(C128S) mice were generated by crossing Tph2-tTA mice with tetO-ChR(C128S)-EYFP knock-in mice under control of the tryptophan hydroxylase 2(Tph2) promoter [43, 57]. Eight bi-genic and six wild-type (WT) C57BL/6J male mice (age > 12 w.o.) were used in this study. Mice were housed at 24 ◦C. on a inverted dark:light cycle (lights on 10:00-22:00, GMT+9). After stereotaxic surgery, mice underwent habituation training [66], MRI experiments, and a reward delay task in turn.

Stereotaxic surgery

Mice were initially sedated with 1-3% isoflurane, and were administered three types of mixed anesthetic agents (1 (mg/mL) of medetomidine, 5.0 (mg/mL) of midaloram, and 5.0 (mg/mL) of butorphanol, i.p.) [21]. Cranial skins were removed with a sterilized surgical knife, and a plastic bar (3x3x27mm) for head-fixation in the MRI environment and an optic fiber (480 µm diameter, 4 mm length, Doric Lenses) was fixed to their skulls with dental acrylic cement. The optical fiber was inserted horizontally toward the DRN from the cerebellum in each mouse. Mice were housed separately after surgery and underwent at least a 1-week recovery period. Mice were habituated to the MRI environment for at least another week. They subsequently underwent imaging sessions.

Acclimation

In order to habituate awake mice to the MRI imaging protocol, an acclimation protocol was applied to the mice after the surgeries for head-fixation [1, 66] . Mice were fixed in a mock MRI environment and exposed to MRI imaging sounds and blue illumination for 2 h to habituate them to a leak of illumination during scanning (2.0 Hz). Acclimation to sounds and illumination was repeated 7 days prior to the first imaging session. Following imaging sessions, at least 3 days acclimation were permitted.

Functional magnetic resonance imaging (fMRI)

Each animal was placed in the MRI animal bed. T2-weighted structural imaging and three T2* functional imaging sessions were performed. MRI images were acquired with

an 11.7-tesla MRI scanner for small animals (Biospec 117/11 system, Bruker Biospin, EmbH, Ettlingen, Germany) with a cryogenic quadrature RF surface probe (Cryoprobe, Bruker BioSpin AG, Fällanden, Switzerland). We performed T2-weighted structural imaging with a RARE sequence with subsequent parameters: 140 x 140 matrix, 13.5 x 13.5 mm2 field-of-view, repetition time(TR)/effective echo time(TE) 4000/18.75 (ms), 31 coronal slices, slice thickness: 300 µm.

After T2-weighted structural imaging was performed, a functional MRI session was further executed. A functional MRI session was composed of two imaging runs, a blue-yellow light stimulation run and a yellow-light stimulation run. All functional imaging was performed using a GE-EPI sequence with following parameters: 67 x 67 matrix, 13.5 x 13.5 mm2 field-of-view, TR/TE 1000/10.7 (ms), flip angle: 50◦, bandwidth: 333k(Hz), 31 coronal slices and slice thickness: 300 µm, and 690 repetitions.

ON/OFF stimulation paradigm

A stimulation protocol was composed of ON/OFF stimulation patterns (Figure 1d). In each activation session, stimulation was initiated 90 volumes after the onset of an imaging session. DRN serotonin neurons were stimulated with blue illumination (490 nm, 3.0 mW, 1.0 sec), and stimulation subsequently ceased with yellow illumination (630 nm, 3.0 mW, 1.0 sec) 20 seconds after the onset of blue illumination. This stimulation was repeated 5 times for 120 seconds after the onset of blue illumination. For the control session, instead of blue illumination, only yellow illumination was applied in stimulation sessions.

Preprocessing and de-noising

The first 10 volume images of each session were removed from subsequent analysis due to initial imaging instability caused by motion and non-steady state image quality. 10-fold magnification of images was done to process images with Statistical Parametric Mapping 12 (SPM12), which is designed to process human brain images. Therefore, the voxel size was 2 x 2 x 3 mm in analytical steps. Pre-processing, including motion correction, realignment, co-registration, normalization to a C57BL6/J template [18], and spatial smoothing (kernel with 3 x 3 x 6 mm) was executed with Statistical Parametric Mapping (SPM12). Since each slice of a 3D brain image was taken at a different time, slice timing correction was applied to correct slice-timing differences by temporal interpolation. Next, realignment of 3D brain images was conducted to correct motion-related changes of brain position. Then, co-registration was executed to overlay functional T2* images onto structural T2 images and to save coordination changes of T2* images for normalization. During normalization, T2 structural images were first warped to fit the average C57BL6/J template [18]. Then T2* functional images were further warped to the template using the co-registered coordination change of the images. In spatial smoothing, voxel signals were spatially smoothed using a gaussian kernel (4 x 4 x 6 mm). After pre-processing steps, the general linear model in SPM12 was executed to map spatial activation patterns.

Regions of Interest

The Allen brain institute provides a parcellation of the C57BL6 mouse brain. In order to extract BOLD signals from anatomically defined brain regions, this parcellation was

utilized for subsequent analyses. Parcellation was first warped to the MRI template using Advanced Normalization Tools (ANTs), and 28 regions of interest (ROIs) were selected from the warped parcellation. 28 ROIs were selected with the following three criteria. First, primary cortical regions, especially mid-line regions, were selected. Second, primary reward- and punishment-related sub-cortical regions, including basal ganglia, VTA, and DRN should were included. Third, ventro-lateral cortical and sub-cortical regions, such as the amygdala complex were not selected due to its sensitivity to artifacts near air cavities by the ear canals [24].

General Linear Model (GLM) for BOLD signals

A general linear model (GLM) was performed to map beta values of parameter estimation of optogenetic stimulation onto the mouse brain template with SPM12. For statistical functional mapping of optogenetic stimulation, each voxel under an uncorrected P value < 0.001 was thresholded, and cluster-wise multiple comparisons were subsequently executed with family-wise error (©) by thresholding pFWE < 0.05 with probabilistic threshold-free cluster enhancement (pTFCE) [56]. Statistical second-level voxel-wise analysis was finally executed to compare functional maps of blue and yellow illumination from transgenic mice. For session 1, all procedures were executed accordingly. For sessions 2, 3, and 4, none of the voxels under uncorrected P values < 0.001 survived the thresholding.

Beta values from BOLD responses

Furthermore, regional beta values were extracted based on ROIs. Statistical significance of regional beta values was subsequently tested with Student's t tests with multiple comparisons with the false discovery rate (FDR; p value (FDR) < 0.05). Each regional BOLD signal change (%) is calculated by averaging regional time series on voxels, which are scaled with the mean of time series during the no-stimulation period and followed with multiplication by 100.

Structural density and RNA expression maps

The structural density map of serotonin connections was obtained from the mouse brain database of the Allen Brain Institute (Experimental IDs: 480074702) [17]. As with the structural density map, gene expression of serotonin receptors was obtained from the mouse brain database of Allen Brain Institute (Experimental IDs: 79556616 (5HT1a), 583 (5HT1b), 69859867 (5HT1f), 81671344 (5HT2a), and 73636098 (5HT2c)). Normalized energy intensity was extracted from the normalized atlas. Multiple linear model analysis of ROIs between betas from GLM analyses and gene expressions was performed.

Multivariable Linear Regression Model (MLRM)

Beta values from each session were obtained based on 28 ROIs. Structural density and RNA expression of 5HT1a, 1b, 1f, 2a, and 2c was also extracted based on 28 ROIs. Multivariable linear models were used to estimate weights of structural and gene expression of 5HT receptors; where beta values from each session were the dependent variables, and intensity of structural and gene expression was the explanatory variable. The results of statistical values for fitting are described in Table 2.

One-way Analysis of Variance (ANOVA) on Receptor Contribution

Regression coefficients of structural density and RNA expression of 5-HT receptors were calculated for each subject for all sessions. One-way ANOVA was applied to regression coefficients of each receptor type in order to test whether receptor expression is statistically different between awake (sessions 1, 2, &4) and anesthetized states (session 3). For the analysis, data from all sessions were concatenated (total data: n=29, session 1 (awake): n=8; session 2(awake): n=7, session 3 (anesthetized): n=7, session 4 (awake): n=7). p values from one-way ANOVA were further corrected with the Bonferroni method. Results of ANOVA are described in Supplementary Table ST3.

A reward delay task

After imaging sessions, some mice from both groups (Transgenic: n=3, WT: n=2) subsequently performed a waiting experiment for a delayed reward. A sequential tone-food waiting task was utilized for a free operant task [37, 39] (Supplementary Figure S1a). After MRI sessions, individual subjects were trained and tested in an operant-conditioning box (Med-Associates, 12.7x12.7 cm). In short, subjects were required to initiate trials by nose-poking into a tone site 500 (ms). The reward-delay task was composed of reward trials (75%) and omission trials (25%). We adopted two types of stimulation protocols (Supplementary Figure S1b): fixed-delay and random-delay protocols. At the onset of reward and omission trials, either blue or yellow illumination was delivered. In the reward trials, blue/yellow light stimulation was delivered at the onset of each trial until nose-poking was performed, and yellow light was delivered when subjects waited for 6.0 (s) for the fixed protocol and 2, 6, or 10 (s) for the random delay protocol. However, yellow illumination was also given when subjects failed to wait for the delay. On the other hand, during omission trials, yellow stimulation was given when mice gave up waiting for delayed rewards while light stimulation was delivered in the same manner as in the reward trials.

Data and code availability

Raw data including functional and structural images will be available soon. Codes and pre-processed data are also available from https://github.com/Taiyou/OptofMRI_5HT. All software used in this study is also available (Supplementary Table ST1)

Acknowledgments

We thank Dr. Koji Toda (Keio University) for his comments on awake optogenetic stimulation, Dr. Keigo Hikishima for his comments on fMRI, Mr. Yoshiaki Ohba for creation of acclimation tools, and DMD. Jiafu Zeng for animal support for MRI acquisition.

Author contributions

HTH and KD conceived the experiments. HTH, AY, NT designed and prepared experiments, HTH performed MRI experiments. MT conducted behavioral experiments. HTH analysed results, and HTH wrote the manuscript. All authors reviewed the manuscript.

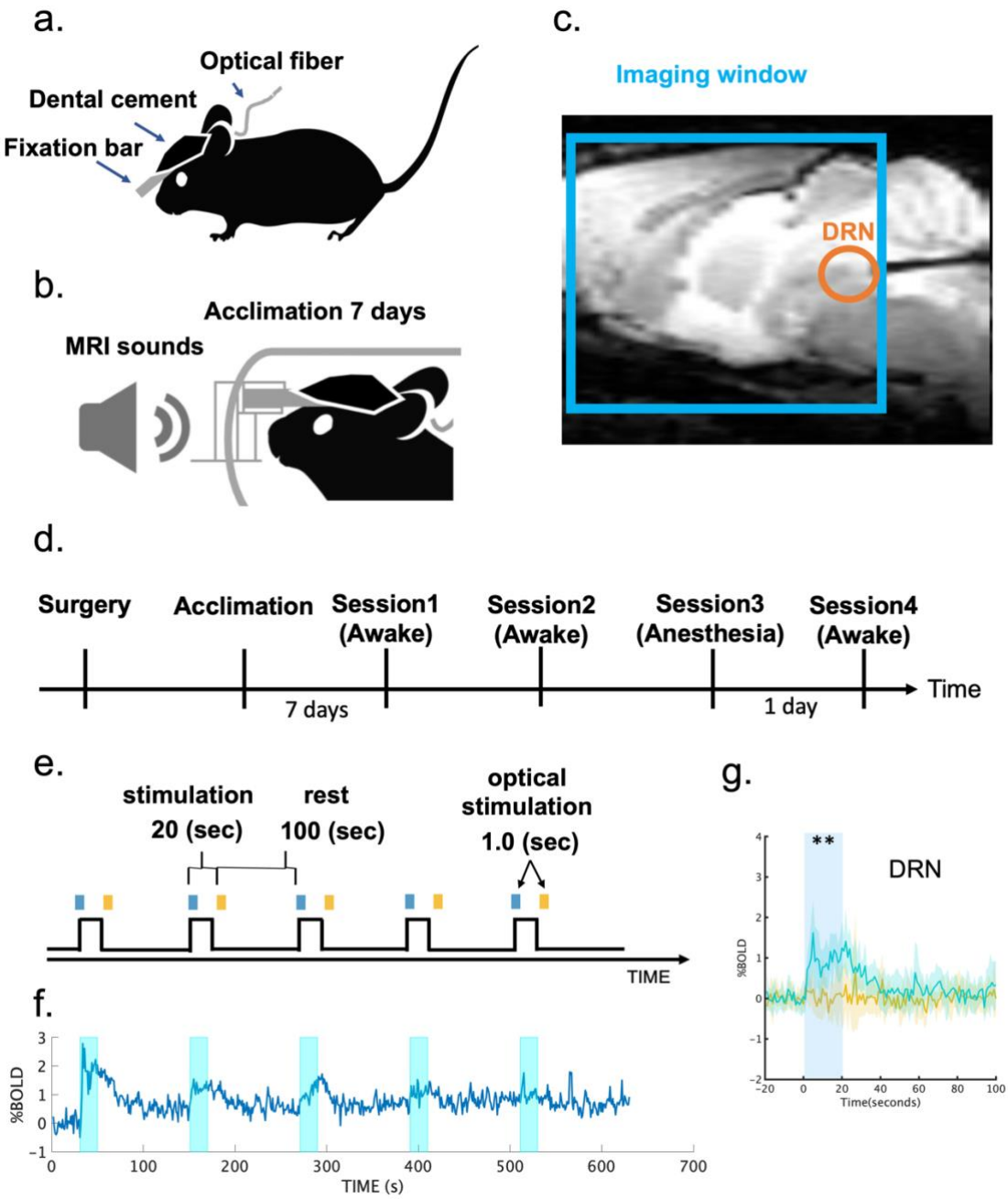

Figure 1. (a) Surgical setup. A fixation bar was mounted on the mouse head with dental cement and an optical cannula was inserted into the dorsal raphe nucleus (DRN) (b) Acclimation protocol. A mouse was exposed daily to recorded MRI scanning sounds for 2 h for 7 days prior to fMRI sessions. (c) Location of an optical cannula. An optical cannula was inserted horizontally into the DRN from the cerebellum. A cyan window indicates the imaging window for T2* sessions. (d) Experimental schedule. After surgery and 7 days acclimation, the first fMRI recording session was performed. A replication session was also performed a few weeks later. Finally, experiments for anesthesia effects were performed. On the 1st day, an fMRI recording with general anesthesia using isoflurane 1% was performed, and an fMRI recording without anesthesia was conducted thereafte©(e) Stimulation protocol. In an fMRI session, the onset of optogenetic stimulation was applied 90 s after an imaging session began. Blue illumination (1.0 s; 473 nm) was applied at the onset of stimulation, and yellow illumination (1.0 second; 593 nm) followed the offset of stimulation 20 s after blue illumination. (f) Average time course of % BOLD signals in DRN. Time

series of % BOLD signals were individually extracted from the DRN in session 1 and session 2, and the time series were averaged across transgenic mice (n = 8). Each cyan window indicates the stimulation period during a session for 20 s. (g) Alignment of average % BOLD responses in the DRN. % BOLD responses were aligned at the time of blue illumination (1.0 s) in session 1. Blue and yellow lines indicate % BOLD responses in the DRN from blue and yellow stimulation sessions from the transgenic group (n = 8), respectively. A cyan window indicates stimulation duration during a session for 20 s.

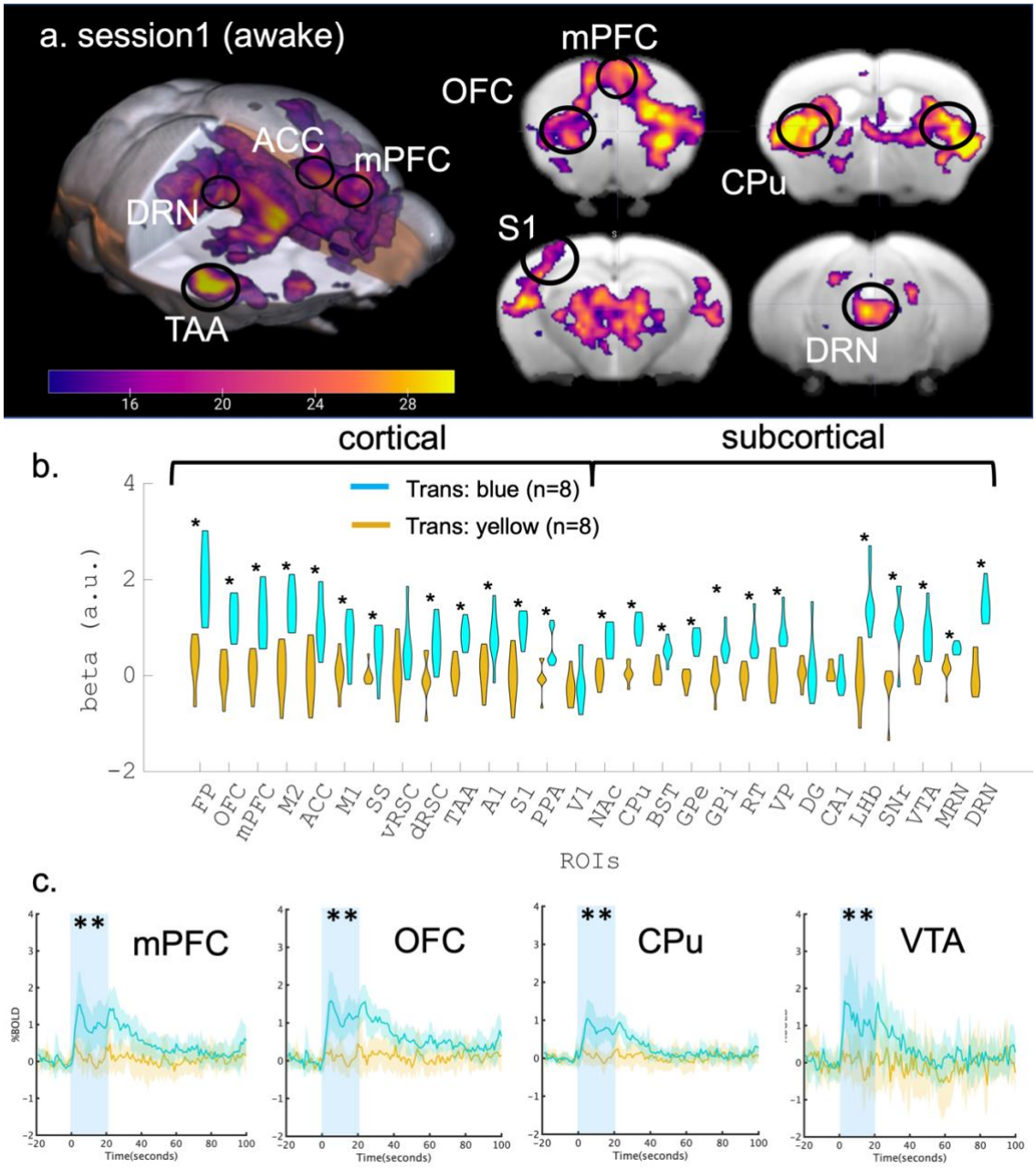

Figure 2. (a) Functional map of optogenetic illumination. A functional map was calculated by contrasting BOLD responses between blue and yellow illumination in the transgenic (n = 8) group ($p < 0.05$, cluster-corrected controlling family-wise e©r (FWE) with probabilistic threshold-free cluster enhancement (pTFCE, see 'General Linear Model (GLM) for BOLD signals' in the Method section)). Magenta color indicates the t value. (b) Comparison of beta values in multiple ROIs. Beta values were obtained from GLM analysis in session 1, and were extracted and averaged based on ROIs from the Allen Brain Atlas (Table 1). Differences of beta values between blue and yellow illumination sessions were contrasted in the transgenic group. * indicates $p<0.05$ (multiple comparison was corrected with false discovery rate (FDR)). Cyan and magenta colors indicate blue and yellow illumination, respectively. (c) Alignment of average % BOLD responses in mPFc, OFC, CPu, and VTA. % BOLD responses were aligned at the time of blue illumination (1.0 s) in session 1. Blue illumination (1.0 s; 473 nm) was applied at the onset of stimulation, and yellow illumination (1.0 second; 593 nm) followed 20 s the offset of the stimulation after blue illumination. A cyan window indicates stimulation duration during a session for 20 s. Blue and yellow lines indicate % BOLD responses in mPFc, OFC, CPu, and VTA from blue and yellow illumination from

transgenic groups (n = 8), respectively. A cyan window indicates stimulation duration during a session for 20 s.

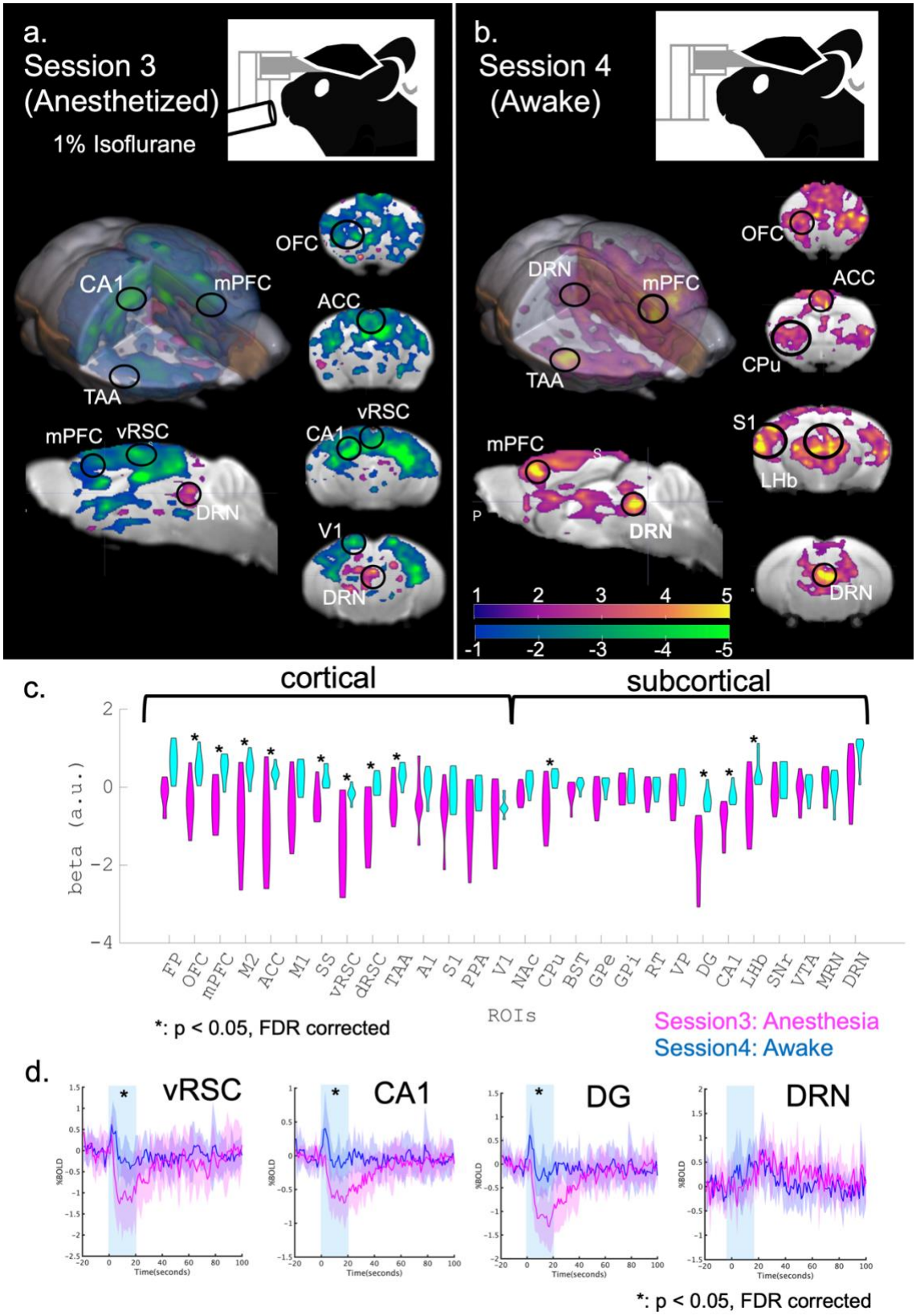

Figure 3. (a) Optogenetic fMRI session with general anesthesia in session 3. General anesthesia, 1% isoflurane, was applied to the transgenic group (n=7) during optogenetic fMRI sessions. GLM analysis following optogenetic stimulation was executed and visualized (T > 1, uncorrected). Magenta and cyan

colors indicate positive and negative statistical t values. (b) An optogenetic fMRI session in the awake state in session 4. As in session 1, no anesthesia was applied to the transgenic group during optogenetic fMRI sessions. As on day 1, GLM analysis was executed and visualized (T > 1, uncorrected). (c) Comparison between beta values of sessions 3 and 4 in multiple ROIs. Beta values of blue illumination sessions in session 3 and session 4 were statistically contrasted using Student's t test. * indicates $p<0.05$, FDR-corrected. (d) Alignment of average % BOLD responses in vRSC, CA1, DG, and DRN in session 3 from transgenic mice. Blue illumination (1.0 s; 473 nm) was applied at the onset of stimulation, and yellow illumination (1.0 second; 593 nm) followed the offset of stimulation 20 s after the blue illumination. A cyan window indicates stimulation duration for 20 seconds. * indicates $p<0.05$, FDR corrected.

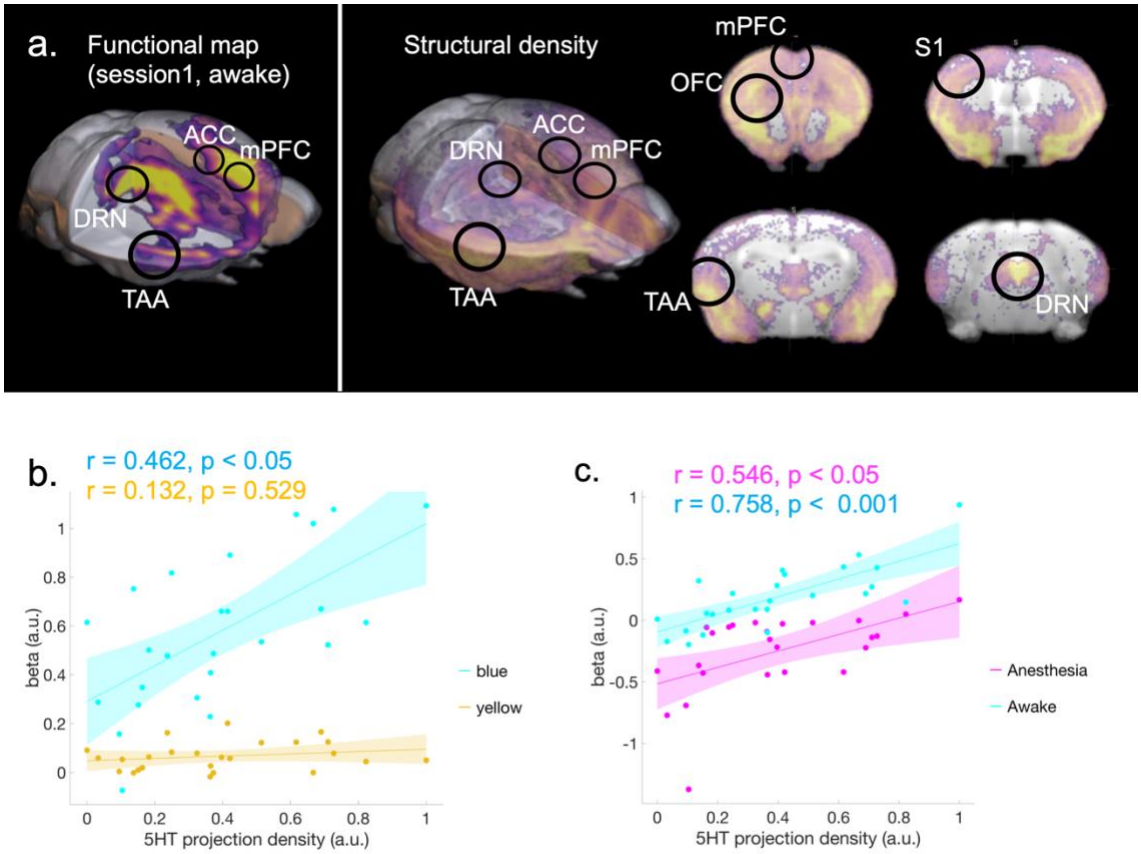

Figure 4. (a) Structural density map of serotonergic projection. A structural density map of serotonergic projections was obtained from the Allen Brain Atlas. (b) Correlation between projection density and regional beta values. The correlation between regional structural density and average regional beta values across transgenic groups was calculated from session 1 (blue stimulation: $r = 0.462$, $p < 0.05$; yellow stimulation: $r = 0.132$, $p = 0.529$, FDR corrected). Blue and yellow colors indicate data from blue and yellow illumination sessions, respectively. (c) Correlation between projection density and regional beta values. The correlation between regional structural density and average regional beta values across transgenic groups was calculated (Anesthetized (Session3): $r = 0.546$, $p < 0.05$; Awake (Session4): $r = 0.758$, $p < 0.001$, FDR corrected). Magenta and blue colors indicate data from blue illumination sessions in sessions 3 and 4, respectively.

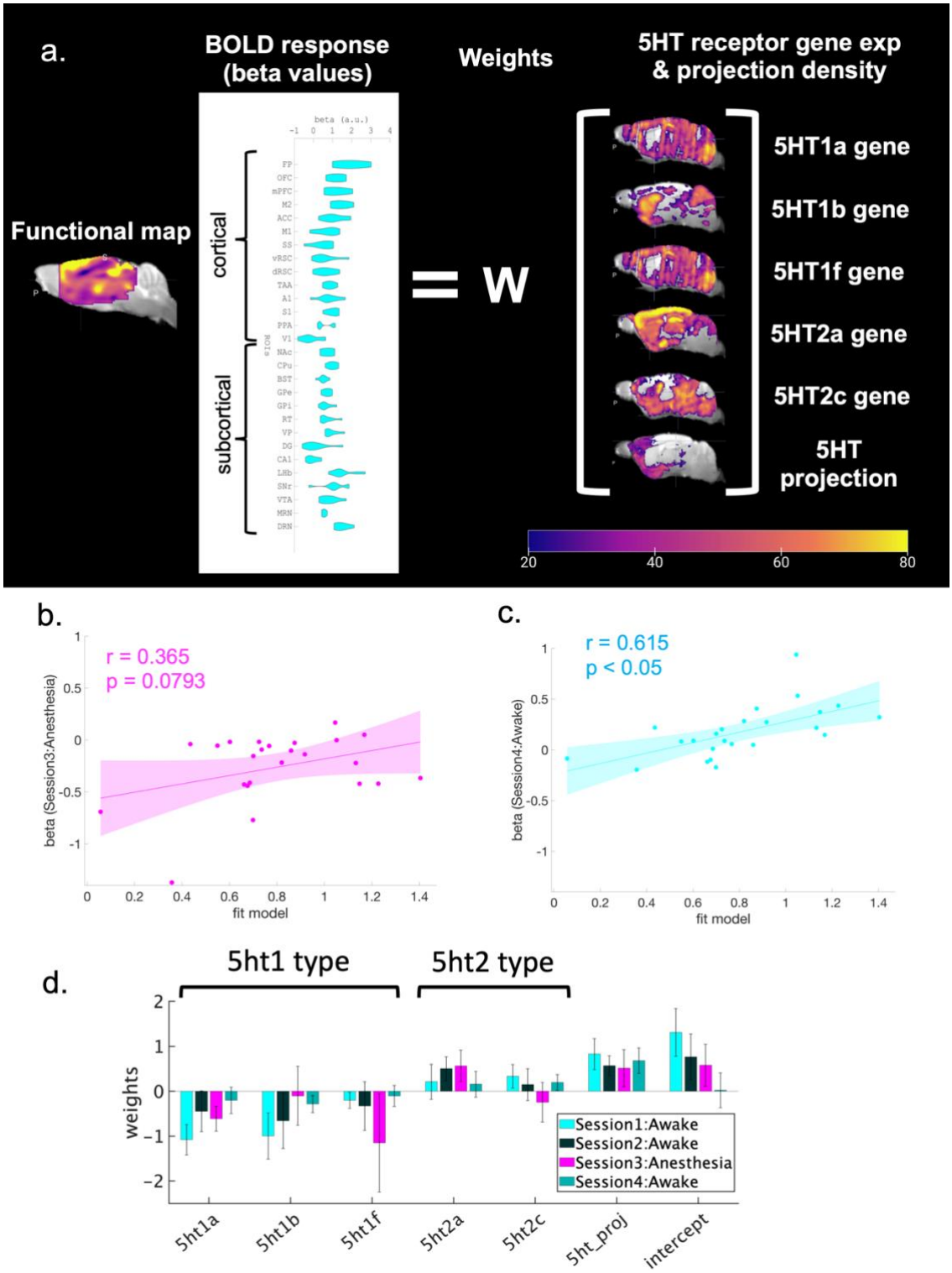

Figure 5. (a) Procedure to make a model of predicted beta values in session 1 of blue illumination. Independent variables, including regional structural densities and regional gene expression of 5ht1a, 5ht1b, 5ht1f, 5ht2a, and 5ht2c were fit with a linear regression model to beta values of multiple ROIs from blue illumination sessions. (b) Correlation between modeled beta values from session 1 and beta values from session 3 under anesthesia ($r = 0.365$, $p = 0.079$, FDR corrected). (c) Correlation between modeled beta values from session 1 and beta values from session 4 (Awake: $r = 0.615$, $p < 0.01$, FDR corrected). (d) Weights of fitted models from session 1, session 2, and session 3 under anesthesia, and session 4 without

anesthesia. Cyan, black, magenta, and green colors indicate weights of expression profiles from session 1 (n=8), session2 (n=7), session 3 (n=7) and session 4 (n=7), respectively.

ROI id	Area	ROI name	Abbreviations
1	Cortical regions	Frontal polar area	FP
2		Orbital area	OFC
3		Medial prefrontal cortex	mPFC
4		Secondary motor area	M2
5		Anterior cingulate cortex	ACC
6		Primary motor area	M1
7		Supplementary somatosensory area	SS
8		Ventral retrosplenial cortex	vRSC
9		Dorsal retrosplenial cortex	dRSC
10		Temporal association area	TAA
11		Primary auditory area	A1
12		Primary somatosensory area	S1
13		Posterior parietal association area	PPA
14		Primary visual area	V1
15	Sub-cortical regions	Nucleus accumbens	NAc
16		Caudate putamen	CPu
17		Bed nucleus of steria terminalis	BST
18		Globus pallidus external part	GPe
19		Globus pallidus internal part	GPi
20		Thalamic reticular nucleus	RT
21		Ventral pallidus	VP
22		Dentate gyrus of hippocampus	DG
23		CA1 of hippocampus	CA1
24		Lateral habenula	LHb
25		Substantia nigra pars reticulata	SNr
26		Ventral tegmental area	VTA
27		Medial raphe nucleus	MRN
28		Dorsal raphe nucleus	DRN

Table1. Regions of interest (ROIs) and their abbreviations. ROIs are ordered from anterior to posterior for cortical and subcortical areas.

Model Statistics (Session 1)				
	R^2 statistic	F-statistic	P value (uncorrected)	Estimate of the error variance
Session 1	0.6603	5.5063	0.0025	0.0643

Table 2. Model with Parameter Estimate of Session 1. Multiple linear regression was performed to fit parameter estimates from session 1 (blue stimulation) with density of serotonergic projection and expression of 5-HT receptors.

		SS	df	MS	F-statistic	p value
5-ht1a						
	Group	0.00111	1	0.00111	0	0.945
	Error	6.20697	27	0.22989		
	Total	6.20808	28			
5-ht1b						
	Group	1.6679	1	1.66795	5.07	0.0327
	Error	8.8794	27	0.32886		
	Total	10.5473	28			
5-ht1f						
	Group	4.6674	1	4.66744	12.95	**0.0013***
	Error	9.7293	27	0.36034		
	Total	14.4967	28			
5-ht2a						
	Group	0.40786	1	0.40786	3.43	0.075
	Error	3.21128	27	0.11894		
	Total	3.61914	28			
5-ht2c						
	Group	10.103	1	10.103	31.08	**0.0019***
	Error	8.779	27	0.3251		
	Total	18.8809	28			
Structural density						
	Group	0.18596	1	0.18596	1.73	0.1999
	Error	2.90782	27	0.1077		
	Total	3.0938	28			
Intercept						
	Group	0.1135	1	0.11348	0.26	0.6171
	Error	11.9762	27	0.44356		
	Total	12.0896	28			

Table 3. Results of one-way ANOVA for 5-HT receptor type and structural intensity. One-way ANOVA was applied to regression coefficients from each factor to test whether each factor showed statistically different expressions between awake state and anesthetized states. SS, df, and MS indicate Sum of Squares, Degrees of freedom, and Mean Squares, respectively. * indicates statistical significance after multiple correction with the Bonferroni method ($p < 0.05$).

References

1. Abe, Y., et al., Diffusion functional MRI reveals global brain network functional abnormalities driven by targeted local activity in a neuropsychiatric disease mouse model. Neuroimage, 2020. 223: p. 117318.
2. Amargos-Bosch, M., et al., Co-expression and in vivo interaction of serotonin1A and serotonin2A receptors in pyramidal neurons of prefrontal cortex. Cereb Cortex, 2004. 14(3): p. 281-99.
3. Anderson, I.M., et al., Assessing human 5-HT function in vivo with pharmacoMRI. Neuropharmacology, 2008. 55(6): p. 1029-37.
4. Boschert, U., et al., The mouse 5-hydroxytryptamine1B receptor is localized predominantly on axon terminals. Neuroscience, 1994. 58(1): p. 167-82.
5. Boureau, Y.L. and P. Dayan, Opponency revisited: competition and cooperation between dopamine and serotonin. Neuropsychopharmacology, 2011. 36(1): p. 74-97.
6. Caraiscos, V.B., et al., Selective enhancement of tonic GABAergic inhibition in murine hippocampal neurons by low concentrations of the volatile anesthetic isoflurane. J Neurosci, 2004. 24(39): p. 8454-8.
7. Cornea-Hebert, V., et al., Cellular and subcellular distribution of the serotonin 5-HT2A receptor in the central nervous system of adult rat. J Comp Neurol, 1999. 409(2): p. 187-209.
8. Correia, P.A., et al., Transient inhibition and long-term facilitation of locomotion by phasic optogenetic activation of serotonin neurons. Elife, 2017. 6.
9. Eichenbaum, H., Prefrontal-hippocampal interactions in episodic memory. Nat Rev Neurosci, 2017. 18(9): p. 547-558.
10. Fonseca, M.S., M. Murakami, and Z.F. Mainen, Activation of dorsal raphe serotonergic neurons promotes waiting but is not reinforcing. Curr Biol, 2015. 25(3): p. 306-315.
11. Fritze, S., R. Spanagel, and H.R. Noori, Adaptive dynamics of the 5-HT systems following chronic administration of selective serotonin reuptake inhibitors: a meta-analysis. J Neurochem, 2017. 142(5): p. 747-755.
12. Fu, W., et al., Chemical neuroanatomy of the dorsal raphe nucleus and adjacent structures of the mouse brain. J Comp Neurol, 2010. 518(17): p. 3464-94.
13. Garcia-Garcia, A.L., et al., Serotonin inputs to the dorsal BNST modulate anxiety in a 5-HT(1A) receptor-dependent manner. Mol Psychiatry, 2018. 23(10): p. 1990-1997.
14. Giorgetti, M. and L.H. Tecott, Contributions of 5-HT(2C) receptors to multiple actions of central serotonin systems. Eur J Pharmacol, 2004. 488(1-3): p. 1-9.
15. Giorgi, A., et al., Brain-wide Mapping of Endogenous Serotonergic Transmission via Chemogenetic fMRI. Cell Rep, 2017. 21(4): p. 910-918.
16. Grandjean, J., et al., A brain-wide functional map of the serotonergic responses to acute stress and fluoxetine. Nat Commun, 2019. 10(1): p. 350.
17. Harris, J.A., et al., Anatomical characterization of Cre driver mice for neural circuit mapping and manipulation. Front Neural Circuits, 2014. 8: p. 76.

18. Hikishima, K., et al., In vivo microscopic voxel-based morphometry with a brain template to characterize strain-specific structures in the mouse brain. Sci Rep, 2017. 7(1): p. 85.
19. Iigaya, K., et al., An effect of serotonergic stimulation on learning rates for rewards apparent after long intertrial intervals. Nat Commun, 2018. 9(1): p. 2477.
20. Izquierdo, I., C.R. Furini, and J.C. Myskiw, Fear Memory. Physiol Rev, 2016. 96(2): p. 695-750.
21. Kawai, S., et al., Effect of three types of mixed anesthetic agents alternate to ketamine in mice. Exp Anim, 2011. 60(5): p. 481-7.
22. Klomp, A., et al., Lasting effects of chronic fluoxetine treatment on the late developing rat brain: age-dependent changes in the serotonergic neurotransmitter system assessed by pharmacological MRI. Neuroimage, 2012. 59(1): p. 218-26.
23. Li, A., et al., Dorsal raphe serotonergic neurons promote arousal from isoflurane anesthesia. CNS Neurosci Ther, 2021. 27(8): p. 941-950.
24. Li, R., et al., Restoring susceptibility induced MRI signal loss in rat brain at 9.4 T: A step towards whole brain functional connectivity imaging. PLoS One, 2015. 10(4): p. e0119450.
25. Li, Y., et al., Serotonin neurons in the dorsal raphe nucleus encode reward signals. Nat Commun, 2016. 7: p. 10503.
26. Liu, Z., et al., Dorsal raphe neurons signal reward through 5-HT and glutamate. Neuron, 2014. 81(6): p. 1360-1374.
27. Lottem, E., et al., Activation of serotonin neurons promotes active persistence in a probabilistic foraging task. Nat Commun, 2018. 9(1): p. 1000.
28. Lucaites, V.L., et al., [3H]LY334370, a novel radioligand for the 5-HT1F receptor. II. Autoradiographic localization in rat, guinea pig, monkey and human brain. Naunyn Schmiedebergs Arch Pharmacol, 2005. 371(3): p. 178-84.
29. Malik, R., et al., Top-down control of hippocampal signal-to-noise by prefrontal long-range inhibition. Cell, 2022. 185(9): p. 1602-1617 e17.
30. Marcinkiewcz, C.A., et al., Serotonin engages an anxiety and fear-promoting circuit in the extended amygdala. Nature, 2016. 537(7618): p. 97-101.
31. Massey, C.A., et al., Isoflurane abolishes spontaneous firing of serotonin neurons and masks their pH/CO(2) chemosensitivity. J Neurophysiol, 2015. 113(7): p. 2879-88.
32. Matias, S., et al., Activity patterns of serotonin neurons underlying cognitive flexibility. Elife, 2017. 6.
33. Matsunaga, F., et al., Molecular interactions between general anesthetics and the 5HT2B receptor. J Biomol Struct Dyn, 2015. 33(1): p. 211-8.
34. McDevitt, R.A., et al., Serotonergic versus nonserotonergic dorsal raphe projection neurons: differential participation in reward circuitry. Cell Rep, 2014. 8(6): p. 1857-1869.
35. Mengod, G., et al., 5-HT receptors in mammalian brain: receptor autoradiography and in situ hybridization studies of new ligands and newly identified receptors. Histochem J, 1996. 28(11): p. 747-58.
36. Meyniel, F., et al., A specific role for serotonin in overcoming effort cost. Elife, 2016. 5.

37. Miyazaki, K., et al., Reward probability and timing uncertainty alter the effect of dorsal raphe serotonin neurons on patience. Nat Commun, 2018. 9(1): p. 2048.
38. Miyazaki, K., et al., Serotonergic projections to the orbitofrontal and medial prefrontal cortices differentially modulate waiting for future rewards. Sci Adv, 2020. 6(48).
39. Miyazaki, K.W., et al., Optogenetic activation of dorsal raphe serotonin neurons enhances patience for future rewards. Curr Biol, 2014. 24(17): p. 2033-40.
40. Mo, B., et al., Restraint stress increases serotonin release in the central nucleus of the amygdala via activation of corticotropin-releasing factor receptors. Brain Res Bull, 2008. 76(5): p. 493-8.
41. Nagai, Y., et al., The Role of Dorsal Raphe Serotonin Neurons in the Balance between Reward and Aversion. Int J Mol Sci, 2020. 21(6).
42. Nichols, D.E. and C.D. Nichols, Serotonin receptors. Chem Rev, 2008. 108(5): p. 1614-41.
43. Ohmura, Y., et al., Optogenetic activation of serotonergic neurons enhances anxiety-like behaviour in mice. Int J Neuropsychopharmacol, 2014. 17(11): p. 1777-83.
44. Ohmura, Y., et al., Disruption of model-based decision making by silencing of serotonin neurons in the dorsal raphe nucleus. Curr Biol, 2021. 31(11): p. 2446-2454 e5.
45. Oikonomou, G., et al., The Serotonergic Raphe Promote Sleep in Zebrafish and Mice. Neuron, 2019. 103(4): p. 686-701 e8.
46. Puig, M.V., et al., In vivo excitation of GABA interneurons in the medial prefrontal cortex through 5-HT3 receptors. Cereb Cortex, 2004. 14(12): p. 1365-75.
47. Puig, M.V. and A.T. Gulledge, Serotonin and prefrontal cortex function: neurons, networks, and circuits. Mol Neurobiol, 2011. 44(3): p. 449-64.
48. Pytliak, M., et al., Serotonin receptors - from molecular biology to clinical applications. Physiol Res, 2011. 60(1): p. 15-25.
49. Ren, J., et al., Anatomically Defined and Functionally Distinct Dorsal Raphe Serotonin Sub-systems. Cell, 2018. 175(2): p. 472-487 e20.
50. Ren, J., et al., Single-cell transcriptomes and whole-brain projections of serotonin neurons in the mouse dorsal and median raphe nuclei. Elife, 2019. 8.
51. Riad, M., et al., Somatodendritic localization of 5-HT1A and preterminal axonal localization of 5-HT1B serotonin receptors in adult rat brain. J Comp Neurol, 2000. 417(2): p. 181-94.
52. Schaefer, A., et al., Serotonergic modulation of intrinsic functional connectivity. Curr Biol, 2014. 24(19): p. 2314-8.
53. Scholl, J., et al., Beyond negative valence: 2-week administration of a serotonergic antidepressant enhances both reward and effort learning signals. PLoS Biol, 2017. 15(2): p. e2000756.
54. Sesack, S.R. and A.A. Grace, Cortico-Basal Ganglia reward network: microcircuitry. Neuropsychopharmacology, 2010. 35(1): p. 27-47.
55. Smith, H.R., et al., Dorsal Raphe Serotonin Neurons Mediate CO(2)-Induced Arousal from Sleep. J Neurosci, 2018. 38(8): p. 1915-1925.

56. Spisak, T., et al., Probabilistic TFCE: A generalized combination of cluster size and voxel intensity to increase statistical power. Neuroimage, 2019. 185: p. 12-26.
57. Tanaka, K.F., et al., Expanding the repertoire of optogenetically targeted cells with an enhanced gene expression system. Cell Rep, 2012. 2(2): p. 397-406.
58. Tanaka, S.C., et al., Serotonin differentially regulates short- and long-term prediction of rewards in the ventral and dorsal striatum. PLoS One, 2007. 2(12): p. e1333.
59. Trusel, M., et al., Punishment-Predictive Cues Guide Avoidance through Potentiation of Hypothalamus-to-Habenula Synapses. Neuron, 2019. 102(1): p. 120-127 e4.
60. Wang, H.Y., et al., Frequency-Dependent Block of Excitatory Neurotransmission by Isoflurane via Dual Presynaptic Mechanisms. J Neurosci, 2020. 40(21): p. 4103-4115.
61. Whittington, R.A. and L. Virag, Isoflurane decreases extracellular serotonin in the mouse hippocampus. Anesth Analg, 2006. 103(1): p. 92-8, table of contents.
62. Winegar, B.D. and M.B. MacIver, Isoflurane depresses hippocampal CA1 glutamate nerve terminals without inhibiting fiber volleys. BMC Neurosci, 2006. 7: p. 5.
63. Xu, S., et al., Dorsal Raphe Serotonergic Neurons Control Intertemporal Choice under Trade-off. Curr Biol, 2017. 27(20): p. 3111-3119 e3.
64. Ying, S.W., et al., Isoflurane modulates excitability in the mouse thalamus via GABA-dependent and GABA-independent mechanisms. Neuropharmacology, 2009. 56(2): p. 438-47.
65. Yokoyama, C., et al., Marmoset Serotonin 5-HT1A Receptor Mapping with a Biased Agonist PET Probe 18F-F13714: Comparison with an Antagonist Tracer 18F-MPPF in Awake and Anesthetized States. Int J Neuropsychopharmacol, 2016. 19(12).
66. Yoshida, K., et al., Physiological effects of a habituation procedure for functional MRI in awake mice using a cryogenic radiofrequency probe. J Neurosci Methods, 2016. 274: p. 38-48.

Supplementary materials

Optogenetic activation of dorsal raphe serotonin neurons induces brain-wide activation, including reward-related circuits

Hiro Taiyo Hamada[1,3,*], Yoshifumi Abe[2], Norio Takata[2], Maaskazu Taira[1], Kenji F. Tanaka[2], Kenji Doya[1,*]

[1] Neural Computation Unit, Okinawa Institute of Science and Technology Graduate University, Okinawa, Japan

[2] Department of Neuropsychiatry, Keio University School of Medicine, Tokyo, Japan

[3] Research & Development Department, Araya Inc., Tokyo, Japan

* Correspondence to hamada_h@araya.org, doya@oist.jp

Software List				
IDs	Name	Contributor	Purpose	URLs
1	Statistical Parametric Mapping 12(SPM12)	The Wellcome Centre for Human Neuroimaging, UCL	MRI data analysis	https://www.fil.ion.ucl.ac.uk/spm/
2	MarsBaR region of interest toolbox for SPM		Brain Reference Registration	http://marsbar.sourceforge.net/
3	MRIcroGL	Chris Rorden, Neuropsychology Lab, University of South Carolina	3D visualization of MRI data	https://www.nitrc.org/ projects/mricrogl/
4	Probabilistic Threshold-free Cluster Enhancement (pTFCE) [3]	Tamás Spisák	A cluster-enhancement method	https://spisakt.github.io/pTFCE/
5	Allen Brain Atlas	Allen Brain Institutes	Reference atlas, 5HT projection map, 5HT receptor gene expressions	https://portal.brain-map.org/
6	Templates for In Vivo Mouse Brain [1]	Keigo Hikishima (k-hikishima@ aist.go.jp)	Mouse brain templates for registration and normalization	https:// www.nitrc.org/ projects/tpm_mouse
7	Gramm [2]	Pierre Morel	Visualization of Violin Plotting	https://github.com/piermorel/gramm
8	in-house analysis programs	Neural Computational Unit	Analysis for time series, Behavioral analysis	https://github.com/Taiyou/OptofMRI_5HT
9	MATLAB	MathWorks	Main analyses and data visualization	https://mathworks.com/

Supplementary Table S1. Software employed in this study

ROI id	ROI name	Allen Brain Atlas Name
1	Frontal polar area (FP)	Forntaol pole, layer 1, 2/3, 5, 6a, 6b
2	Orbital area (OFC)	Orbital area, lateral/medial/ventral/ventrolateral part, layer 1, 2/3, 5, 6a, 6b
3	Medial prefrontal cortex (mPFC)	Prelimbic area, layer 1, 2, 2/3, 5, 6a, 6b & Infralimbic area, layer 1, 2, 2/3, 5, 6a, 6b
4	Secondary motor area (M2)	Secondary Motor area, layer 1, 2/3, 5, 6a, 6b
5	Anterior cingulate cortex (ACC)	Anterior cingulate area, layer 1, 2/3, 5, 6a, 6b & Anterior cingulate area, dorsal/ventral part, layer 1, 2/3, 5, 6a, 6b
6	Primary motor area (M1)	Primary motor area, layer 1, 2/3, 5, 6a, 6b
7	Supplementary somatosensory area (SS)	Supplemental somatosensory area, layer 1, 2/3, 4, 5, 6a, 6b
8	Ventral retrosplenial cortex (vRSC)	Retrosplenial area, ventral part, layer 1, 2/3, 4, 5, 6a, 6b
9	Dorsal retrosplenial cortex (dRSC)	Retrosplenial area, dorsal part, layer 1, 2/3, 4, 5, 6a, 6b
10	Temporal association area (TAA)	Temporal association areas, layer 1, 2/3, 4, 5, 6a, 6b
11	Primary auditory area (A1)	Primary auditory are, layer 1, 2/3, 4, 5, 6a, 6b
12	Primary somatosensory area (S1)	Somatosensory area, layer 1, 2/3, 4, 5, 6a, 6b, Primary somatosensory area, layer 1, 2/3, 4, 5, 6a, 6b, Primary somatosensory area, nose/barrel field, layer 1, 2/3, 4, 5, 6a, 6b
13	Posterior parietal association area (PPA)	Posteior parietal association areas, layer 1, 2/3, 4, 5, 6a, 6b
14	Primary visual area (V1)	Primary visual area, layer 1, 2/3, 4, 5, 6a, 6b
15	Nucleus accumbens (NAc)	Nucleus accumbens
16	Caudate putamen (CPu)	Caudoputamen
17	Bed nucleus of steria terminalis (BST)	Bed nuclei of the stria terminalis, anterior/posterior division
18	Globus pallidus external part (GPe)	Globus pallidus, external segment
19	Globus pallidus internal part (GPi)	Globus pallidus, internal segment
20	Thalamic reticular nucleus (RT)	Reticular nucleus of the thalamus
21	Ventral pallidus (VP)	Pallidum, ventral region
22	Dentate gyrus of hippocampus (DG)	Dentate gyrus, molecular/polymorph/granule cell layer/subgranular zone, Dentate gyrus crest, molecular/polymorph/granule cell layer, Dentate gyrus lateral/medial blade, molecular/polymorph/granucle cell layer
23	CA1 of hippocampus (CA1)	Field CA1, stratum lacunosum-moleculare/stratum oriens/pyramidal layer/stratum radiatum
24	Lateral habenula (LHb)	Lateral habenula
25	Substantia nigra pars reticulata (SNr)	Substantia nigra, reticular part
26	Ventral tegmental area (VTA)	Ventral tegmental area
27	Medial raphe nucleus (MRN)	Superior central nucleus raphe, lateral/medial part
28	Dorsal raphe nucleus (DRN)	Dorsal nucleus raphe

Supplementary Table ST2. A list of correspondence between ROIs and names in Allen Brain Atlas

	Session 1	Session 2	Session 3	Session 4
R^2 statistics	0.5851 ± 0.1574	0.5505 ± 0.0863	0.5240 ± 0.1166	0.5437 ± 0.1100
F statistics	5.1849 ± 3.9732	3.6719 ± 1.2474	3.4689 ± 1.6842	3.7058 ± 1.6093
P value	0.0506 ± 0.0774	0.0352 ± 0.0464	0.0599 ± 0.0609	0.0468 ± 0.0570
EEV	0.1252 ± 0.0644	0.1009 ± 0.0224	0.1316 ± 0.0994	0.0630 ± 0.0259

Supplementary Table ST 3. Summary of multiple linear regression with beta values from session1-4. Multiple linear regression was applied to beta values from each subject for all sessions. Each value indicates mean ± standard error of mean.

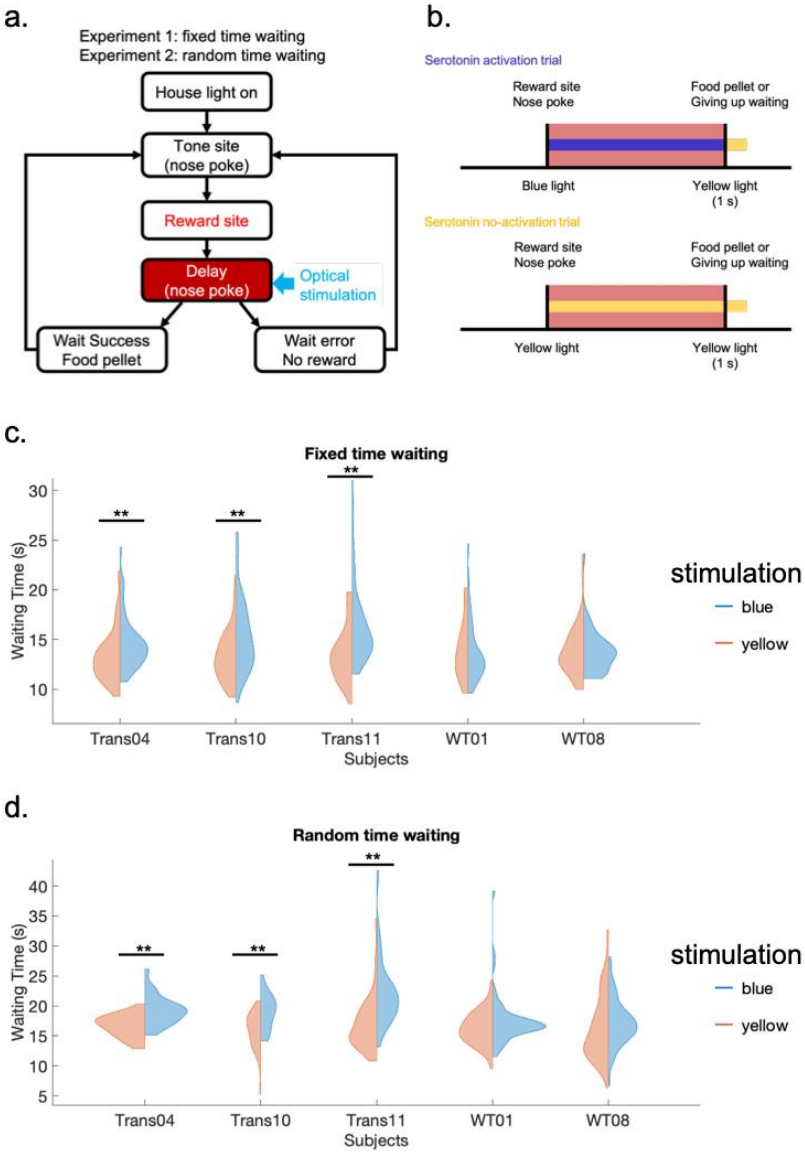

Supplementary Figure S1. (a) Sequence of the tone-food waiting task. (b) Time sequence of optogenetic illumination. In serotonin activation trials, blue light stimulation was delivered until a trial ended with delivery of a food pellet or quitting. In serotonin no—activation trials, yellow light stimulation was delivered until the trial ended. After the trial end, 1 s of yellow light was delivered. Blue and yellow color indicate blue and yellow light stimulation. Red regions indicate reward delay periods. (c) Experiment 1: Fixed time waiting (6.0 s). In this experiment, the reward delay duration for a success trial was fixed at 6 s. For an omission trial, no food reward was given. ** $p < 0.01$ by Wilcoxon rank sum test with Bonferroni correction. Blue and orange regions indicate distributions of blue light and yellow light stimulation. (d) Experiment 2: Random time waiting (2.0, 6.0, or 10.0 s). In this experiment, the reward delay duration for a successful trial was randomly delivered from 2, 6, and 10 s. For an omission trial, no food reward was given to mice. ** $p < 0.01$ by Wilcoxon rank sum test with Bonferroni correction. Blue and orange regions indicate distributions of blue light and yellow light stimulation.

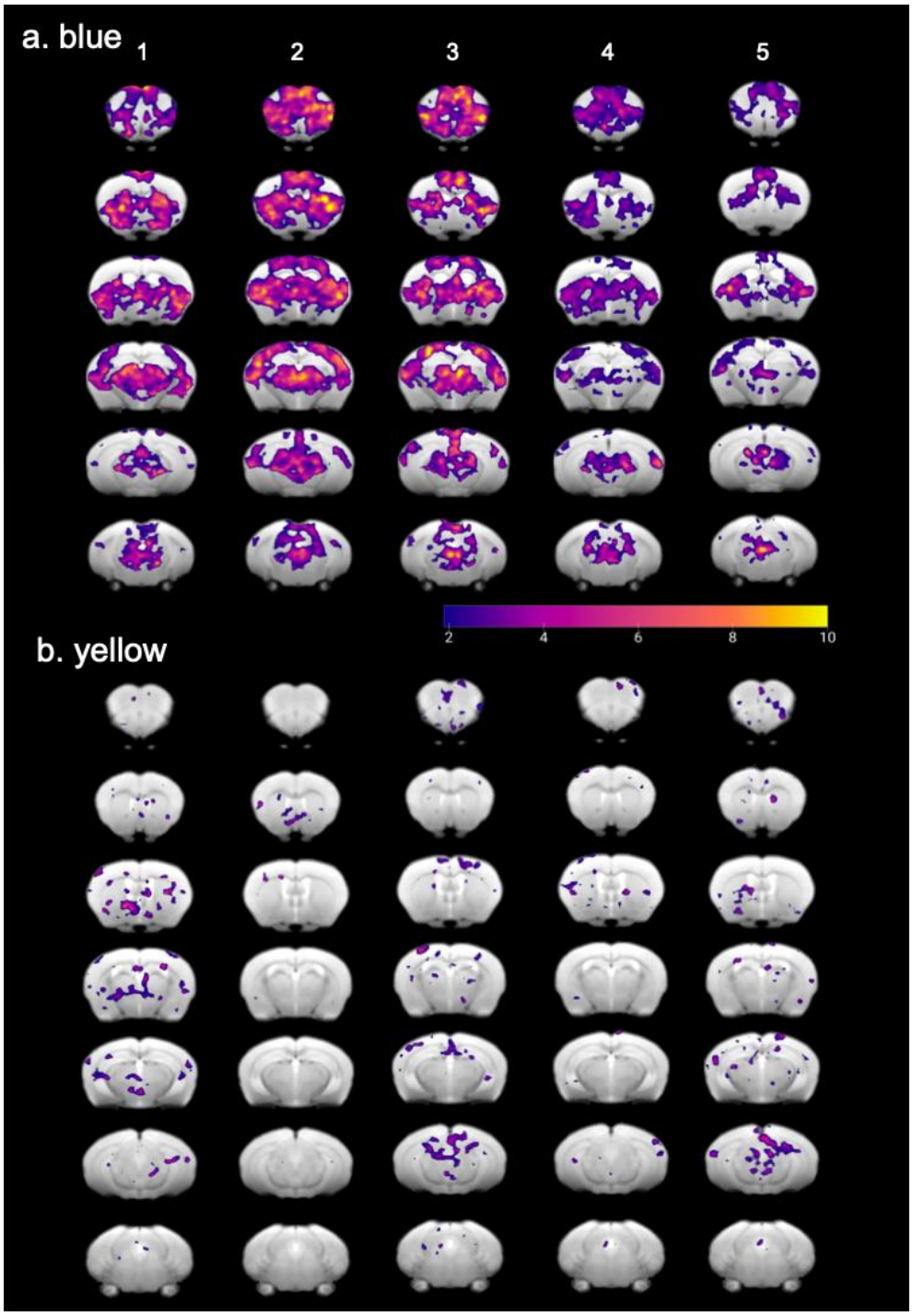

Supplementary Figure S2. (a) Trial-wise functional maps of transgenic mice with blue illumination in session 1 ($p < 0.05$, uncorrected, Transgenic: n = 8). The numbers 1-5 correspond to timing of each stimulus. (b) Trial-wise functional maps of transgenic mice with yellow illumination in session 1 ($p < 0.05$, uncorrected, Transgenic: n = 8).

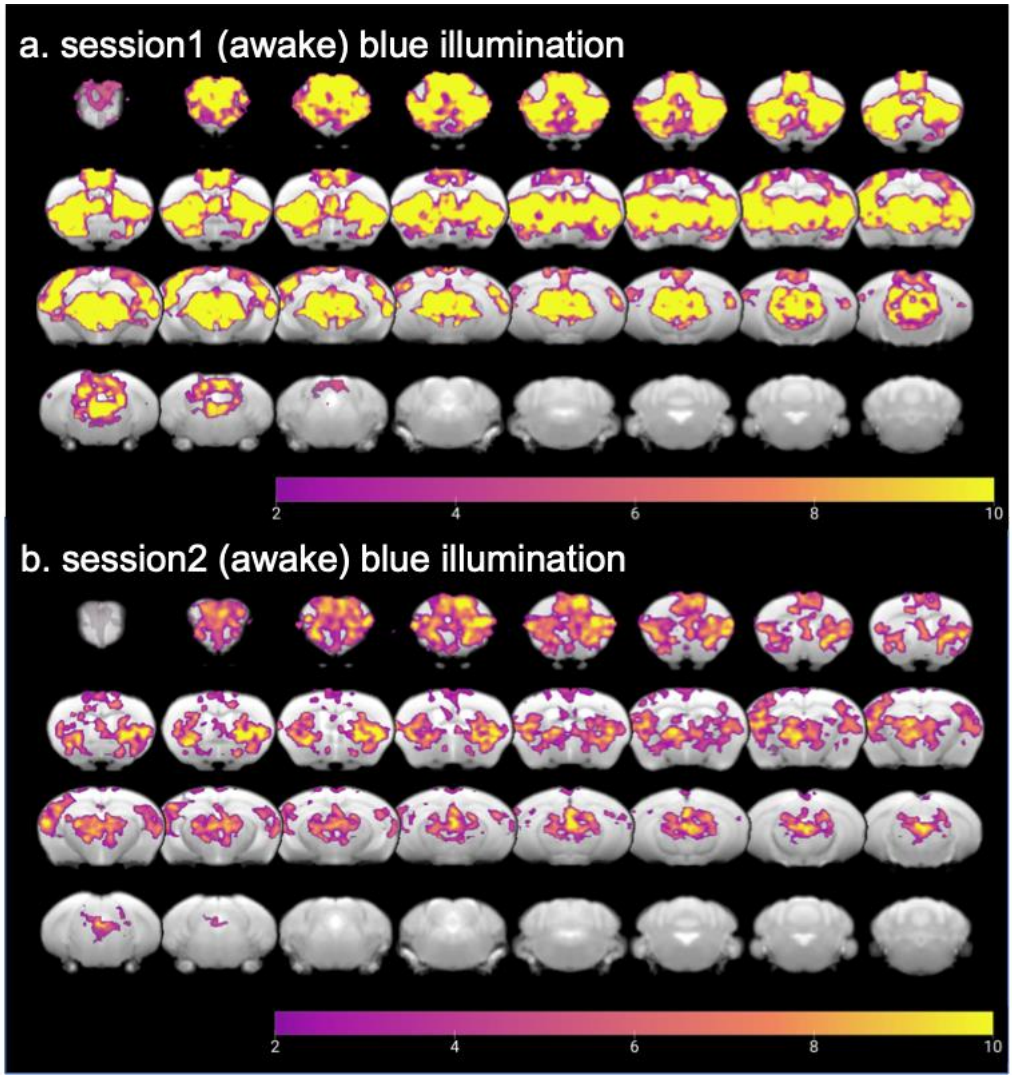

Supplementary Figure S3. (a) Functional map of transgenic mice with blue illumination in session 1 ($p < 0.05$, uncorrected, Transgenic: n = 8). (b) Functional map of transgenic mice with blue illumination in replication session ($p < 0.05$, uncorrected, Transgenic: n = 7).

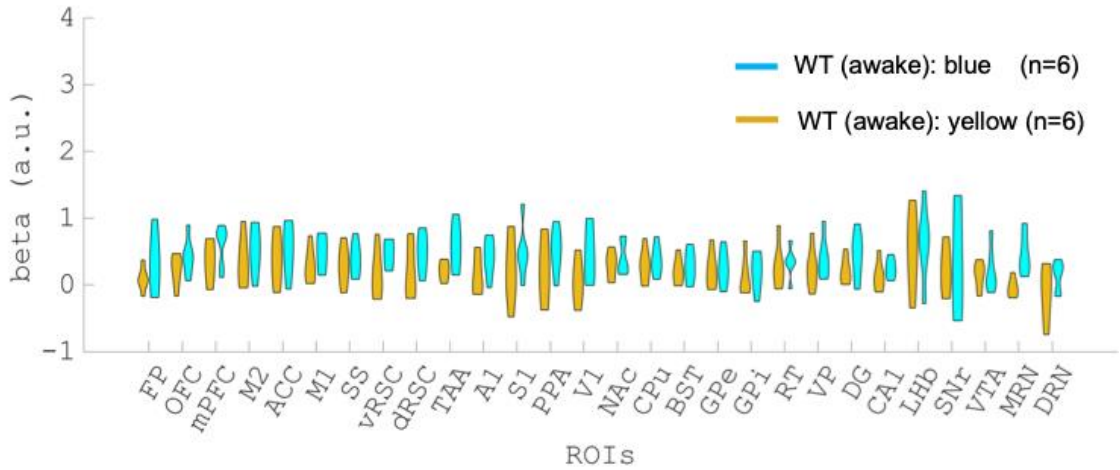

Supplementary Figure S4. Comparison of beta values in multiple ROIs with the WT group (n = 6). Beta values were obtained from GLM analysis in session 1, and were extracted and averaged based on ROIs from the Allen Brain Atlas (Table1.). The difference of beta values between blue and yellow illumination sessions were contrasted in the WT group. Cyan and yellow colors indicate blue and yellow illumination trials, respectively.

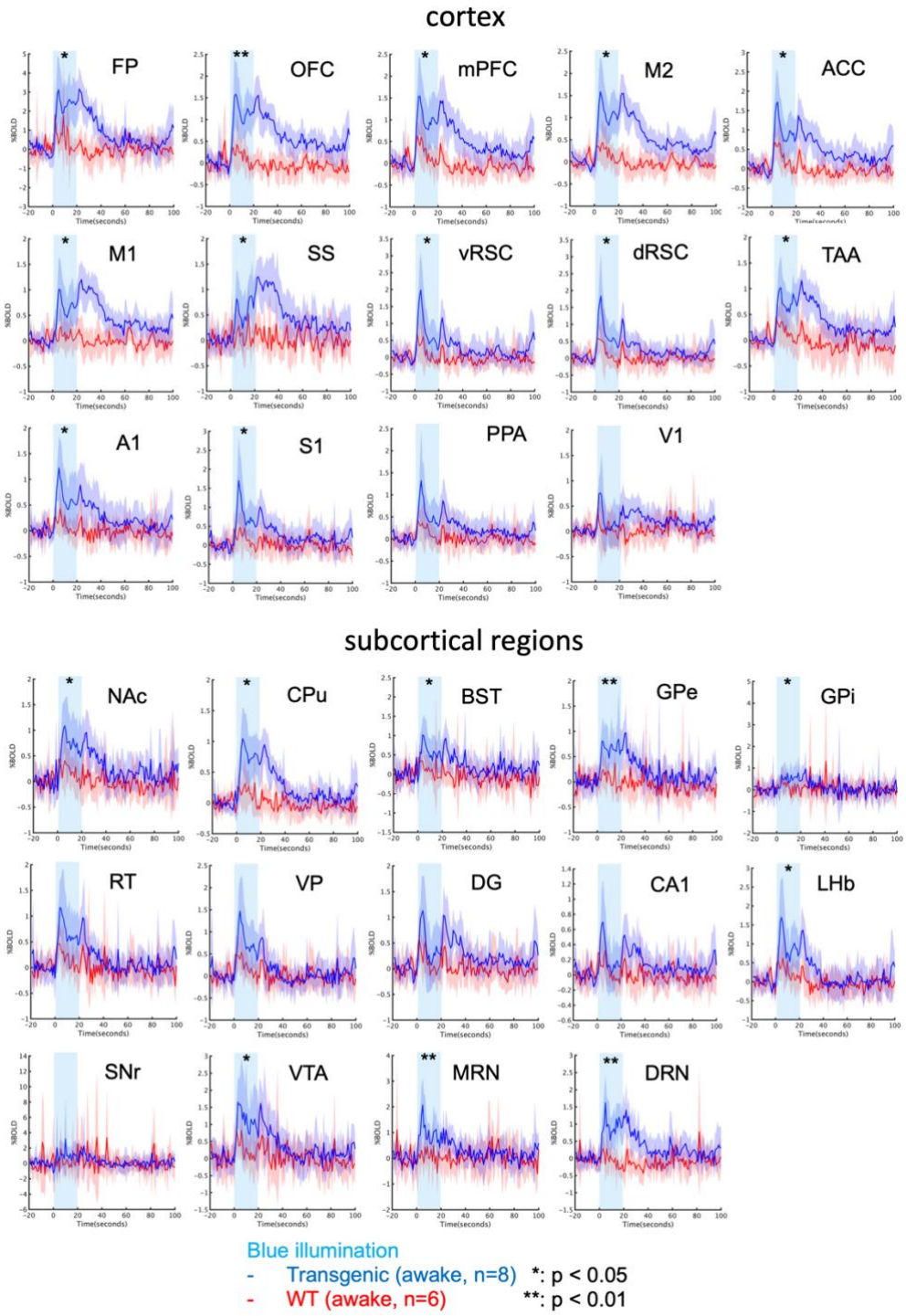

Supplementary Figure S5. Average % BOLD responses to blue illumination in the session 1. Time series of % BOLD responses to yellow illumination in each mouse were averaged at the onset of illumination. Average % BOLD responses were contrasted between the transgenic (n = 8) and WT groups (n = 6). Blue illumination (1.0 s; 473 nm) was applied at the onset of stimulation, and yellow illumination (1.0 second; 593 nm) followed the offset of stimulation 20 s after blue illumination. Cyan highlighting indicates the stimulation duration for 20 s. * and ** indicate statistical p values under 0.05 and 0.01, respectively (corrected with FDR).

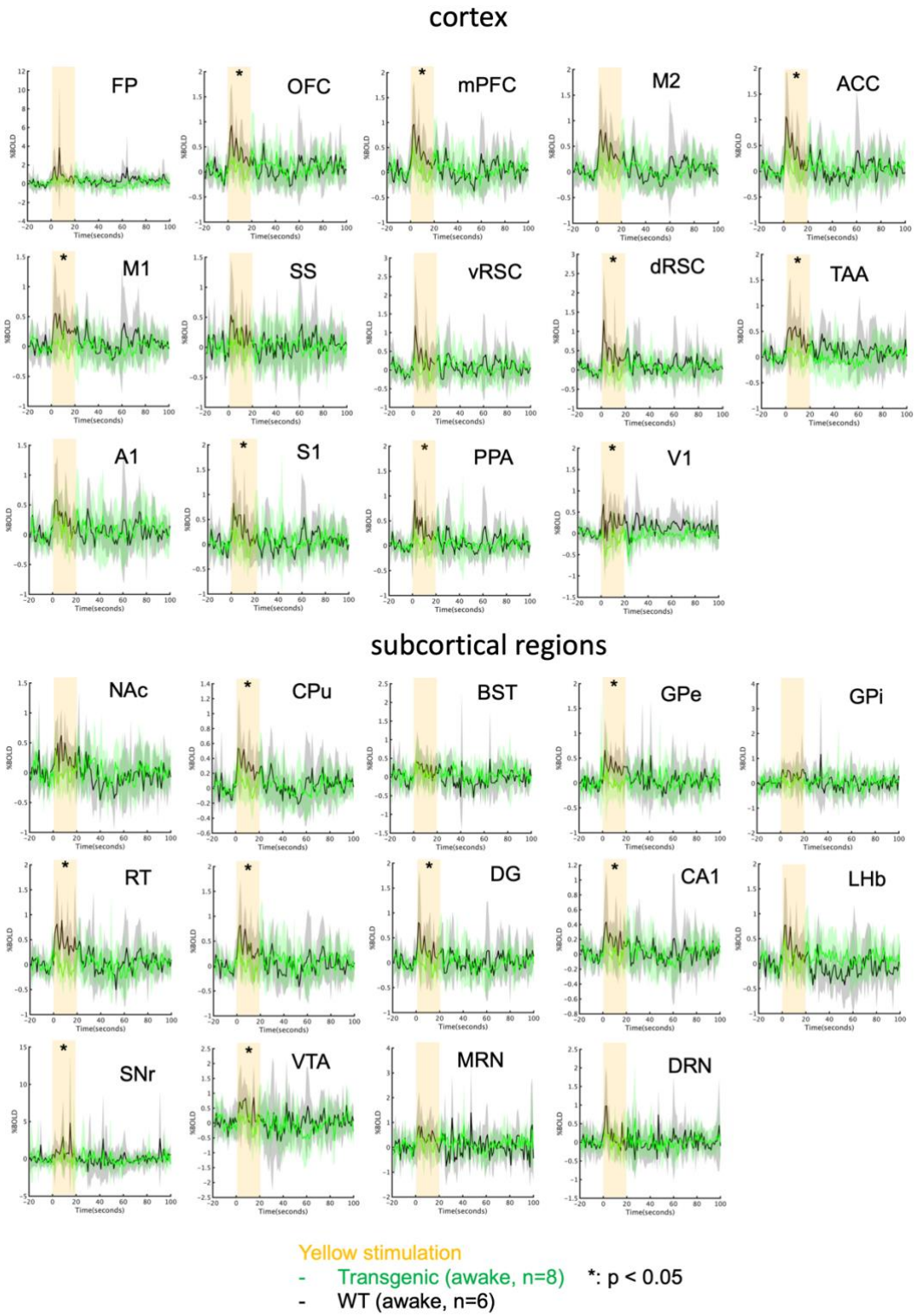

Supplementary Figure S6. Average % BOLD responses of yellow illumination in session 1. Time series of % BOLD responses to yellow illumination in each mouse were averaged at the onset of illumination. Average % BOLD responses were contrasted between the transgenic (n = 8) and WT groups (n = 6). Yellow highlighting indicates the stimulus duration for 20 s. * indicate statistical p values under 0.05 (corrected with FDR).

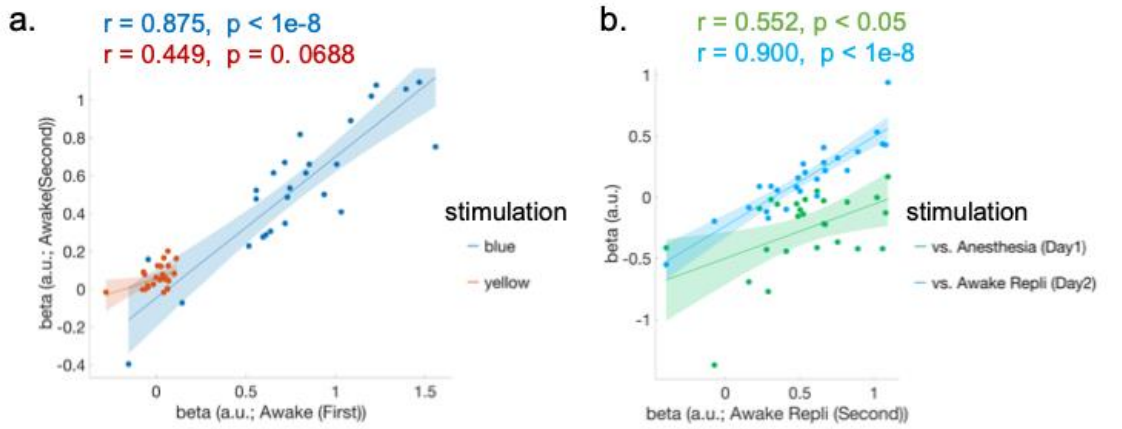

Supplementary Figure S7. (a) Replication of average beta values from GLM to blue stimulation between sessions 1 and 2 in transgenic mice. Statistically significant correlation was found in blue photo-stimulation ($r = 0.875$, $p < 1e-8$), but not in yellow photo-stimulation ($r = 0.449$, $p = 0.0688$). (b) Relationship of average regional beta values from GLM to blue photo-stimulation between session 2 and sessions 3 and 4 in transgenic mice. Statistically significant correlations were found in session 3 under general anesthetics ($r = 0.552$, $p < 0.05$) and in session 4 without general anesthesia ($r = 0.900$, $p < 1e^{-8}$).

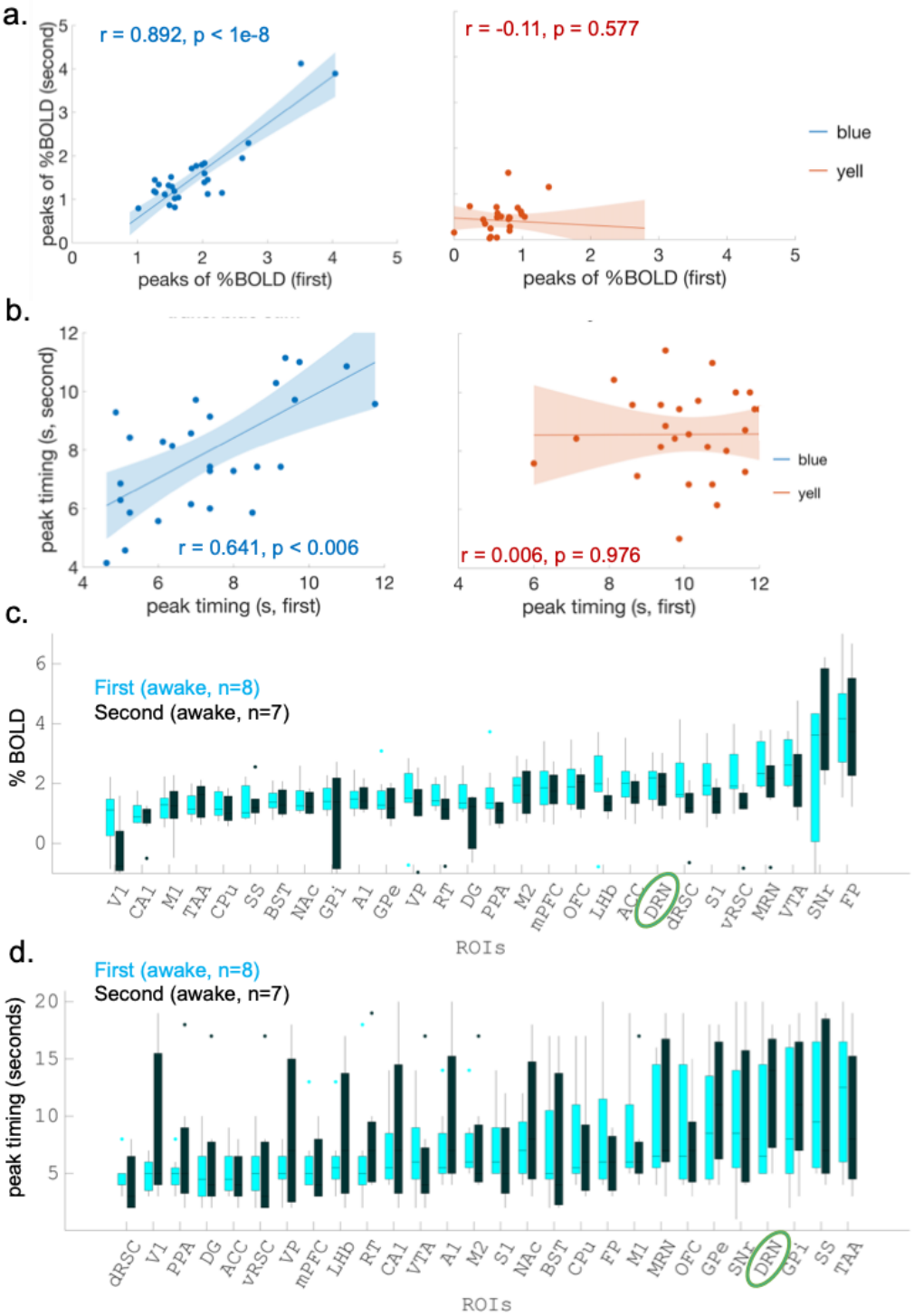

Supplementary Figure S8. (a) Replication of peaks of average % BOLD signals between sessions 1 and 2 in transgenic mice. Statistically significant correlation between peaks of % BOLD responses to blue photo-stimulation in sessions 1 and 2 was found, but not to yellow photo-stimulation (blue illumination: r = 0.8863, p < 1e-8; yellow photo stimulation: r = -0.06, p = 0.766). (b) Replication of peaks of average % BOLD signals between sessions 1 and 2 in transgenic mice. Statistically significant correlation between peak timings of % BOLD responses to blue photo-stimulation in sessions 1 and 2 was found but not to yellow photo-stimulation (blue illumination: r = 0.6785, p < 0.005; yellow photo stimulation: r = 0.0369, p = 0.8551). (c) Alignment of peaks of regional % BOLD signals in sessions 1 and 2. Peaks of % BOLD

signals are sorted in ascending order. (d) Alignment of peak timing of regional % BOLD signals in sessions 1 and 2. Peak timings of regional % BOLD signals are sorted in ascending order.

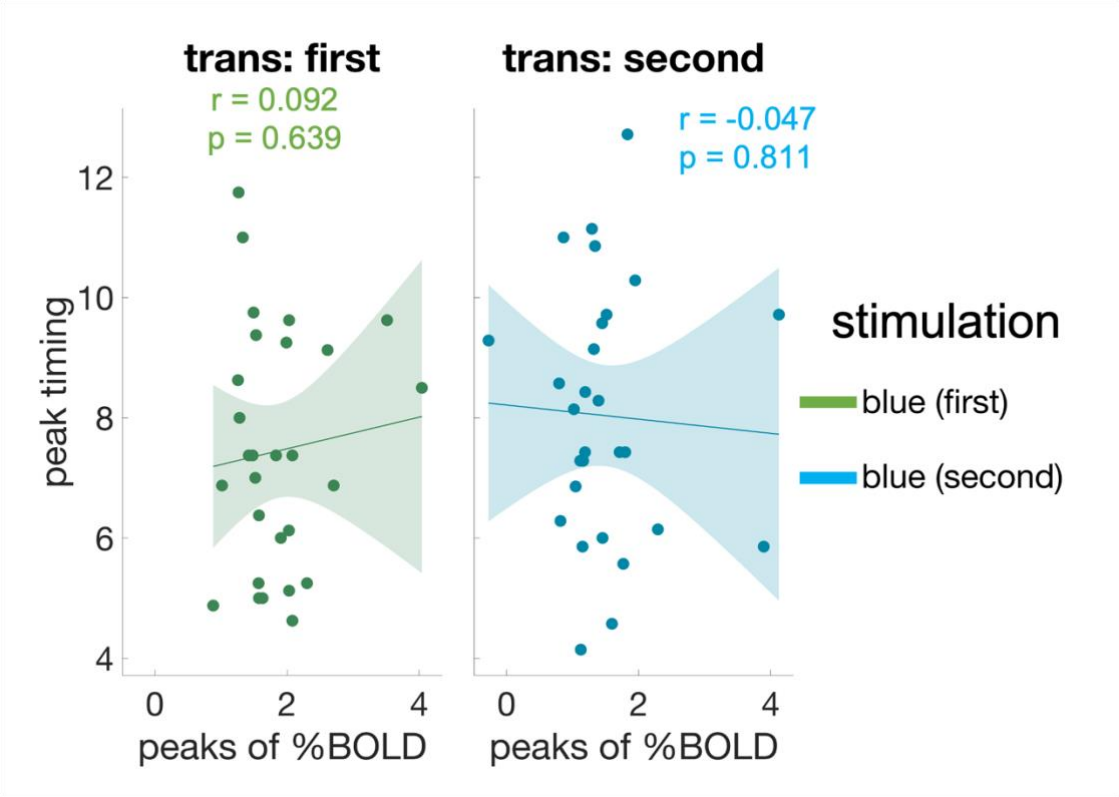

Supplementary Figure S9. Association between peak timing and peaks of average %BOLD signals in sessions 1 and 2. No statistically significant correlations between peak timing and peaks of photo-stimulated %BOLD signals were found in either session (session 1: r = 0.092, p = 0.639; session 2: r = -0.047, p = 0.811).

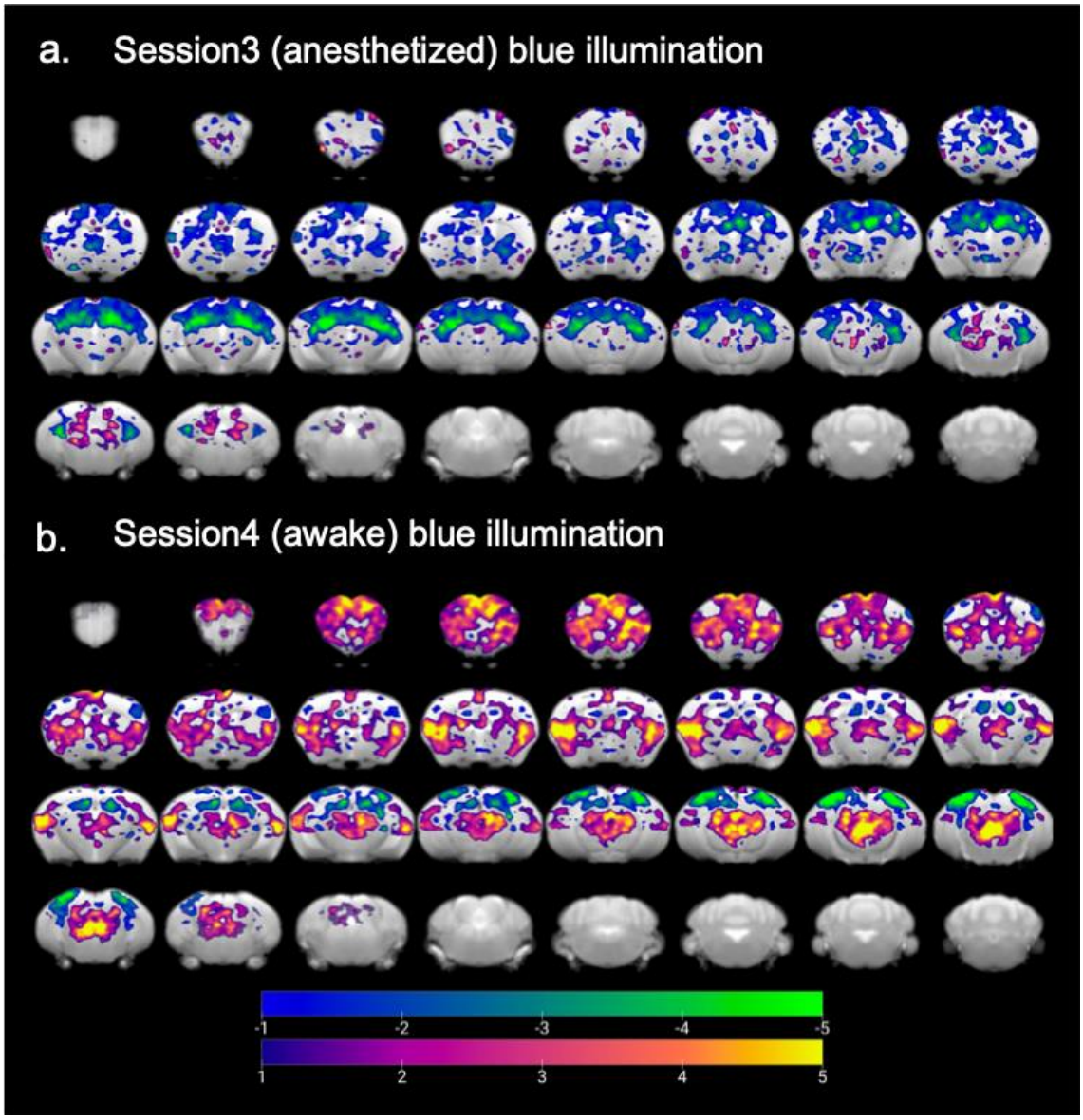

Supplementary Figure S10. (a) Functional map of transgenic mice (n = 7) with blue illumination in session 3 under anesthesia (t > 1, uncorrected). (b) Functional map of transgenic mice (n = 7) with blue illumination in session 4 without anesthesia (t > 1, uncorrected).

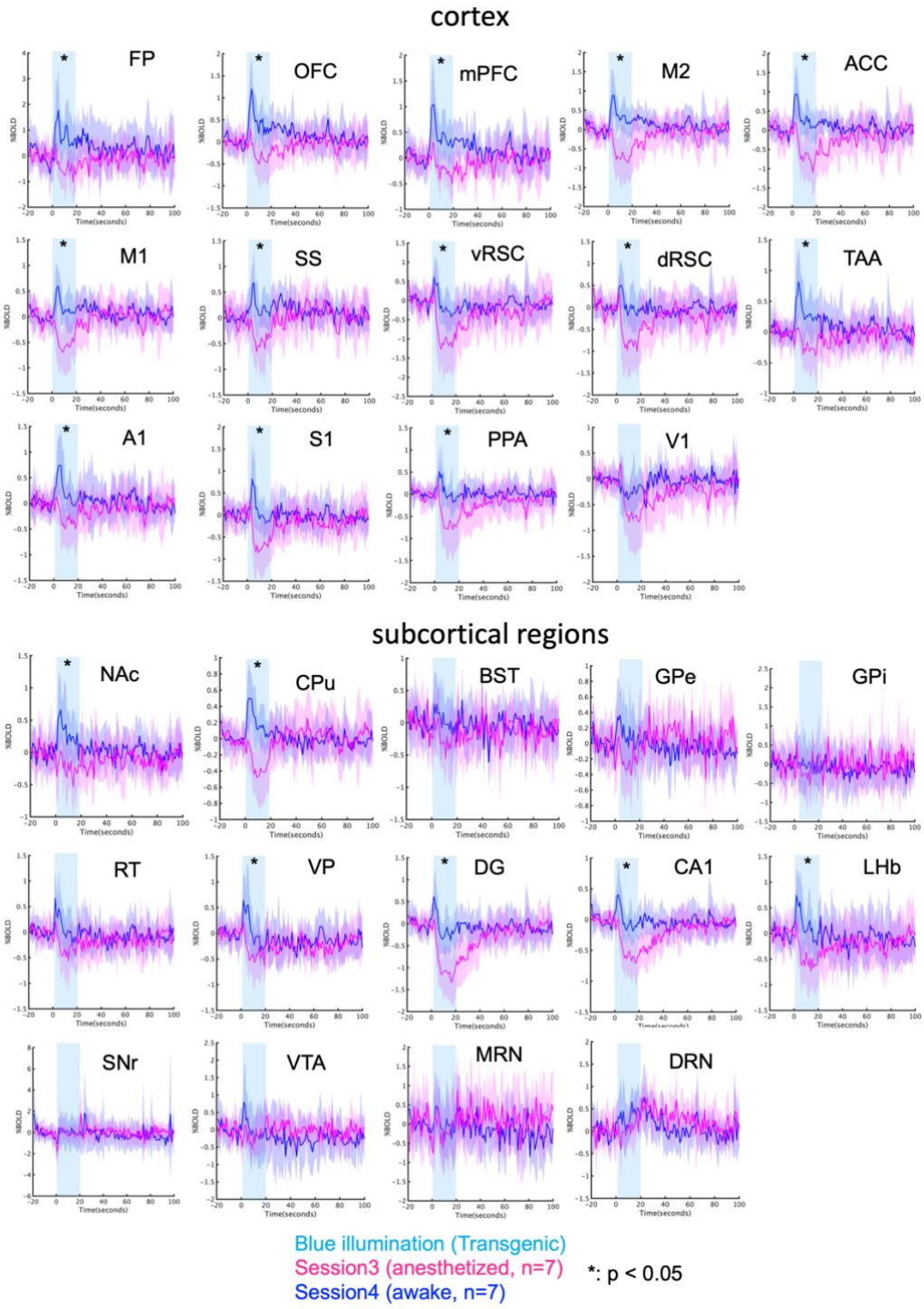

Supplementary Figure S11. Average % BOLD responses to blue illumination in sessions 3 and 4. Time series of % BOLD responses by blue illumination in each mouse were averaged at the onset of illumination. Average % BOLD responses were contrasted between sessions 3 and 4 in the transgenic group (n = 7). Blue illumination (1.0 s; 473 nm) was applied at the onset of stimulation, yellow illumination (1.0 second; 593 nm) followed the offset of stimulation 20 s after blue illumination. Cyan highlighting indicates the stimulus duration for 20 s. * indicate statistical p values under 0.05 (corrected with FDR).

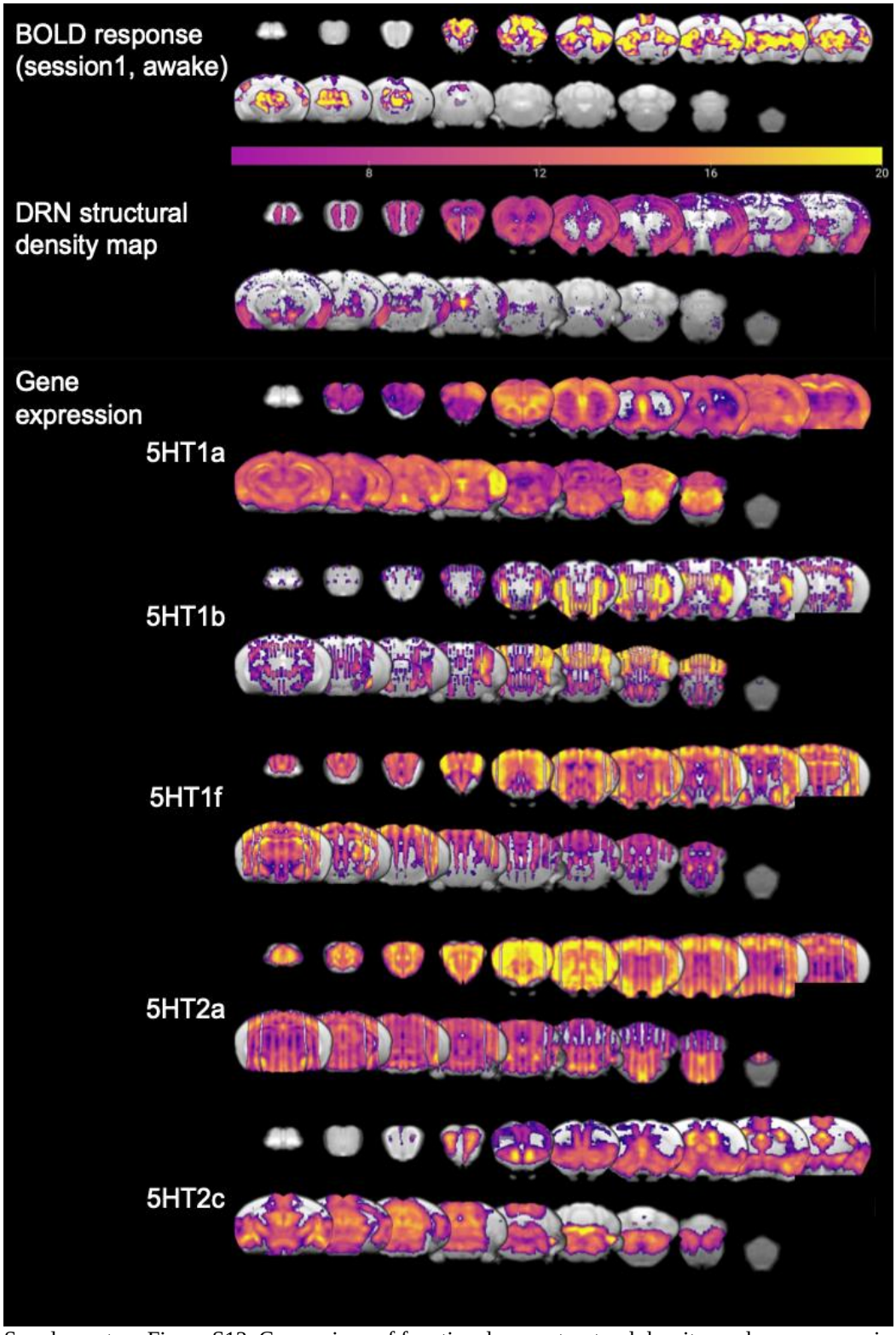

Supplementary Figure S12. Comparison of functional map, structural density, and gene expression maps. The functional map from session 1 under blue illumination was aligned with structural density and gene expression maps. The structural density map and gene expression of serotonin receptors are obtained from the mouse brain database of the Allen Brain Institute (Experimental IDs: 480074702 (5HT projection), 79556616 (5HT1a), 583 (5HT1b), 69859867 (5HT1f), 81671344 (5HT2a), and 73636098 (5HT2c)).

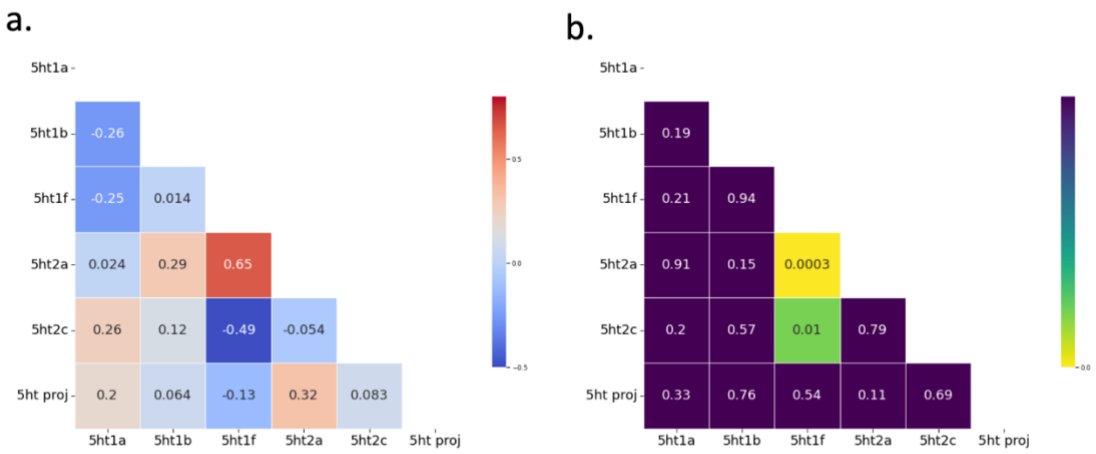

Supplementary Figure S13. Correlation between 5HT projection density and expression profiles of serotonin receptors. (a) Pearson's correlation 5HT projection density and expression profiles of serotonin receptors. (b) Corresponding statistical p values of the correlation between 5HT projection density and expression profiles of serotonin receptors ($p < 0.05$, uncorrected).

References

1. Hikishima, K., et al., In vivo microscopic voxel-based morphometry with a brain template to characterize strain-specific structures in the mouse brain. Sci Rep, 2017. 7(1): p. 85.
2. Morel, P., Gramm: grammar of graphics plotting in Matlab. Journal of Open Source Software, 2018. 3(23): p. 568.
3. Spisak, T., et al., Probabilistic TFCE: A generalized combination of cluster size and voxel intensity to increase statistical power. Neuroimage, 2019. 185: p. 12-26.

Supplementary materials

Optogenetic activation of dorsal raphe serotonin neurons induces brain-wide activation, including reward-related circuits

Hiro Taiyo Hamada[1,3,*], Yoshifumi Abe[2], Norio Takata[2], Maaskazu Taira[1], Kenji F. Tanaka[2], Kenji Doya[1,*]

[1] Neural Computation Unit, Okinawa Institute of Science and Technology Graduate University, Okinawa, Japan

[2] Department of Neuropsychiatry, Keio University School of Medicine, Tokyo, Japan

[3] Research & Development Department, Araya Inc., Tokyo, Japan

* Correspondence to hamada_h@araya.org, doya@oist.jp

Software List				
IDs	Name	Contributor	Purpose	URLs
1	Statistical Parametric Mapping 12(SPM12)	The Wellcome Centre for Human Neuroimaging, UCL	MRI data analysis	https://www.fil.ion.ucl.ac.uk/spm/
2	MarsBaR region of interest toolbox for SPM		Brain Reference Registration	http://marsbar.sourceforge.net/
3	MRIcroGL	Chris Rorden, Neuropsychology Lab, University of South Carolina	3D visualization of MRI data	https://www.nitrc.org/ projects/mricrogl/
4	Probabilistic Threshold-free Cluster Enhancement (pTFCE) [3]	Tamás Spisák	A cluster-enhancement method	https://spisakt.github.io/pTFCE/
5	Allen Brain Atlas	Allen Brain Institutes	Reference atlas, 5HT projection map, 5HT receptor gene expressions	https://portal.brain-map.org/
6	Templates for In Vivo Mouse Brain [1]	Keigo Hikishima (k-hikishima@ aist.go.jp)	Mouse brain templates for registration and normalization	https:// www.nitrc.org/ projects/tpm_mouse
7	Gramm [2]	Pierre Morel	Visualization of Violin Plotting	https://github.com/piermorel/gramm
8	in-house analysis programs	Neural Computational Unit	Analysis for time series, Behavioral analysis	https://github.com/Taiyou/OptofMRI_5HT
9	MATLAB	MathWorks	Main analyses and data visualization	https://mathworks.com/

Supplementary Table S1. Software employed in this study

ROI id	ROI name	Allen Brain Atlas Name
1	Frontal polar area (FP)	Forntaol pole, layer 1, 2/3, 5, 6a, 6b
2	Orbital area (OFC)	Orbital area, lateral/medial/ventral/ventrolateral part, layer 1, 2/3, 5, 6a, 6b
3	Medial prefrontal cortex (mPFC)	Prelimbic area, layer 1, 2, 2/3, 5, 6a, 6b & Infralimbic area, layer 1, 2, 2/3, 5, 6a, 6b
4	Secondary motor area (M2)	Secondary Motor area, layer 1, 2/3, 5, 6a, 6b
5	Anterior cingulate cortex (ACC)	Anterior cingulate area, layer 1, 2/3, 5, 6a, 6b & Anterior cingulate area, dorsal/ventral part, layer 1, 2/3, 5, 6a, 6b
6	Primary motor area (M1)	Primary motor area, layer 1, 2/3, 5, 6a, 6b
7	Supplementary somatosensory area (SS)	Supplemental somatosensory area, layer 1, 2/3, 4, 5, 6a, 6b
8	Ventral retrosplenial cortex (vRSC)	Retrosplenial area, ventral part, layer 1, 2/3, 4, 5, 6a, 6b
9	Dorsal retrosplenial cortex (dRSC)	Retrosplenial area, dorsal part, layer 1, 2/3, 4, 5, 6a, 6b
10	Temporal association area (TAA)	Temporal association areas, layer 1, 2/3, 4, 5, 6a, 6b
11	Primary auditory area (A1)	Primary auditory are, layer 1, 2/3, 4, 5, 6a, 6b
12	Primary somatosensory area (S1)	Somatosensory area, layer 1, 2/3, 4, 5, 6a, 6b, Primary somatosensory area, layer 1, 2/3, 4, 5, 6a, 6b, Primary somatosensory area, nose/barrel field, layer 1, 2/3, 4, 5, 6a, 6b
13	Posterior parietal association area (PPA)	Posteior parietal association areas, layer 1, 2/3, 4, 5, 6a, 6b
14	Primary visual area (V1)	Primary visual area, layer 1, 2/3, 4, 5, 6a, 6b
15	Nucleus accumbens (NAc)	Nucleus accumbens
16	Caudate putamen (CPu)	Caudoputamen
17	Bed nucleus of steria terminalis (BST)	Bed nuclei of the stria terminalis, anterior/posterior division
18	Globus pallidus external part (GPe)	Globus pallidus, external segment
19	Globus pallidus internal part (GPi)	Globus pallidus, internal segment
20	Thalamic reticular nucleus (RT)	Reticular nucleus of the thalamus
21	Ventral pallidus (VP)	Pallidum, ventral region
22	Dentate gyrus of hippocampus (DG)	Dentate gyrus, molecular/polymorph/granule cell layer/subgranular zone, Dentate gyrus crest, molecular/polymorph/granule cell layer, Dentate gyrus lateral/medial blade, molecular/polymorph/granucle cell layer
23	CA1 of hippocampus (CA1)	Field CA1, stratum lacunosum-moleculare/stratum oriens/pyramidal layer/stratum radiatum
24	Lateral habenula (LHb)	Lateral habenula
25	Substantia nigra pars reticulata (SNr)	Substantia nigra, reticular part
26	Ventral tegmental area (VTA)	Ventral tegmental area
27	Medial raphe nucleus (MRN)	Superior central nucleus raphe, lateral/medial part
28	Dorsal raphe nucleus (DRN)	Dorsal nucleus raphe

Supplementary Table ST2. A list of correspondence between ROIs and names in Allen Brain Atlas

	Session 1	Session 2	Session 3	Session 4
R^2 statistics	0.5851 ± 0.1574	0.5505 ± 0.0863	0.5240 ± 0.1166	0.5437 ± 0.1100
F statistics	5.1849 ± 3.9732	3.6719 ± 1.2474	3.4689 ± 1.6842	3.7058 ± 1.6093
P value	0.0506 ± 0.0774	0.0352 ± 0.0464	0.0599 ± 0.0609	0.0468 ± 0.0570
EEV	0.1252 ± 0.0644	0.1009 ± 0.0224	0.1316 ± 0.0994	0.0630 ± 0.0259

Supplementary Table ST 3. Summary of multiple linear regression with beta values from session1-4. Multiple linear regression was applied to beta values from each subject for all sessions. Each value indicates mean ± standard error of mean.

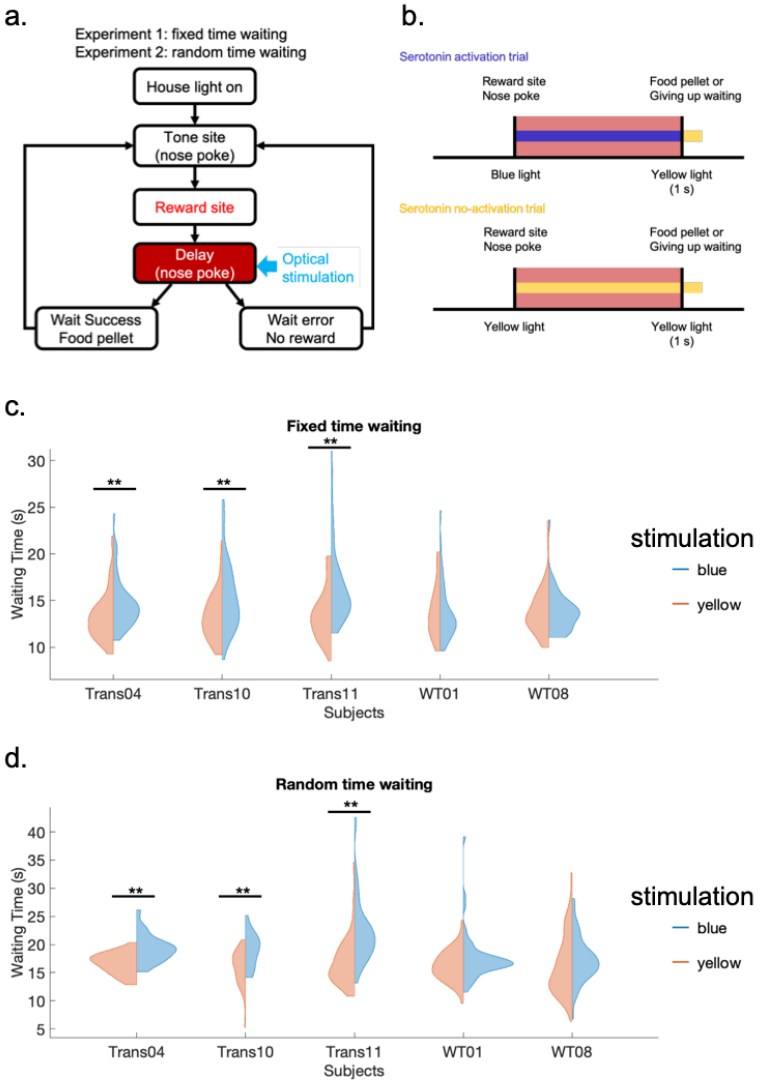

Supplementary Figure S1. (a) Sequence of the tone-food waiting task. (b) Time sequence of optogenetic illumination. In serotonin activation trials, blue light stimulation was delivered until a trial ended with delivery of a food pellet or quitting. In serotonin no—activation trials, yellow light stimulation was delivered until the trial ended. After the trial end, 1 s of yellow light was delivered. Blue and yellow color indicate blue and yellow light stimulation. Red regions indicate reward delay periods. (c) Experiment 1: Fixed time waiting (6.0 s). In this experiment, the reward delay duration for a success trial was fixed at 6 s. For an omission trial, no food reward was given. ** $p < 0.01$ by Wilcoxon rank sum test with Bonferroni correction. Blue and orange regions indicate distributions of blue light and yellow light stimulation. (d) Experiment 2: Random time waiting (2.0, 6.0, or 10.0 s). In this experiment, the reward delay duration for a successful trial was randomly delivered from 2, 6, and 10 s. For an omission trial, no food reward was given to mice. ** $p < 0.01$ by Wilcoxon rank sum test with Bonferroni correction. Blue and orange regions indicate distributions of blue light and yellow light stimulation.

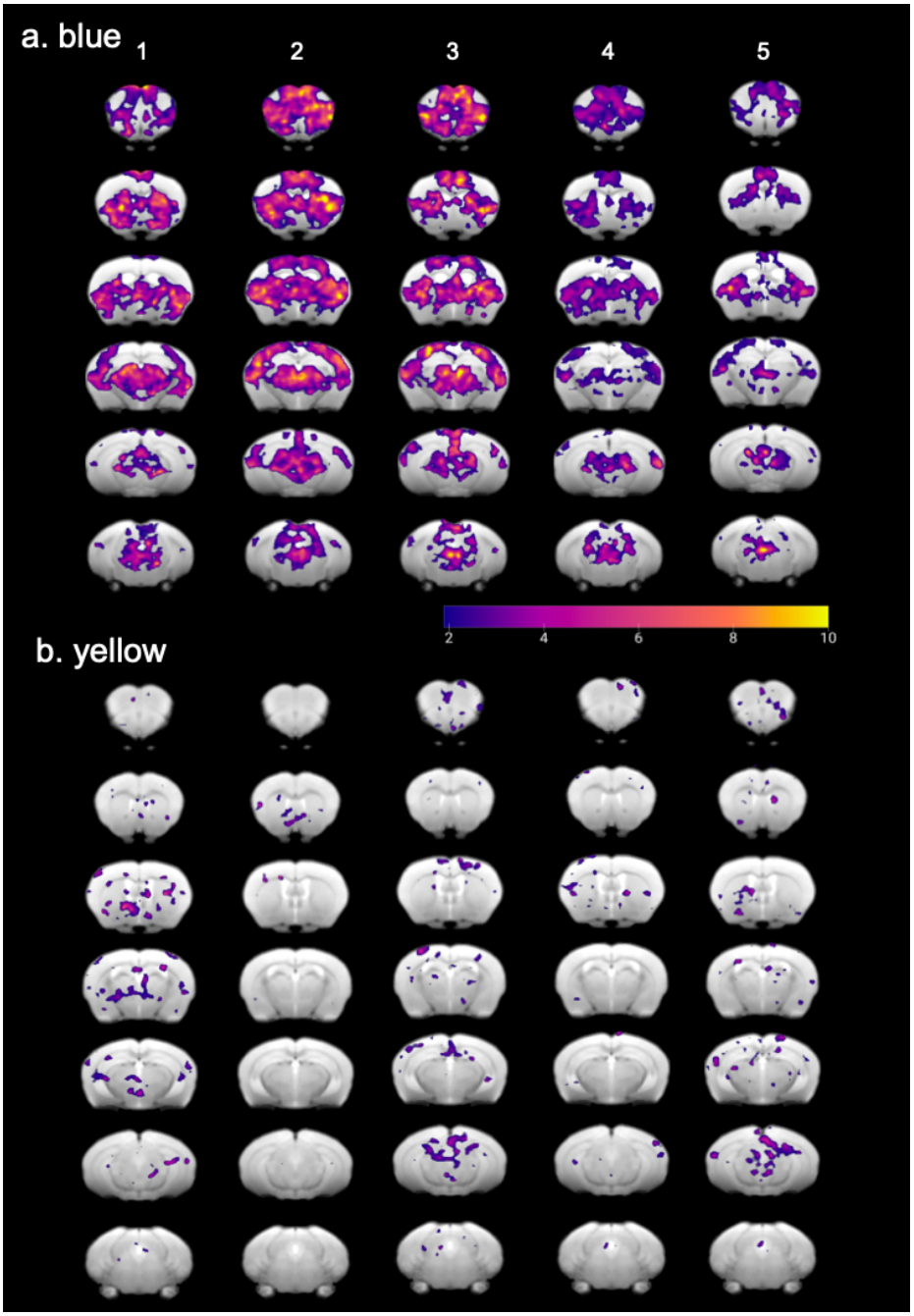

Supplementary Figure S2. (a) Trial-wise functional maps of transgenic mice with blue illumination in session 1 ($p < 0.05$, uncorrected, Transgenic: $n = 8$). The numbers 1-5 correspond to timing of each stimulus. (b) Trial-wise functional maps of transgenic mice with yellow illumination in session 1 ($p < 0.05$, uncorrected, Transgenic: $n = 8$).

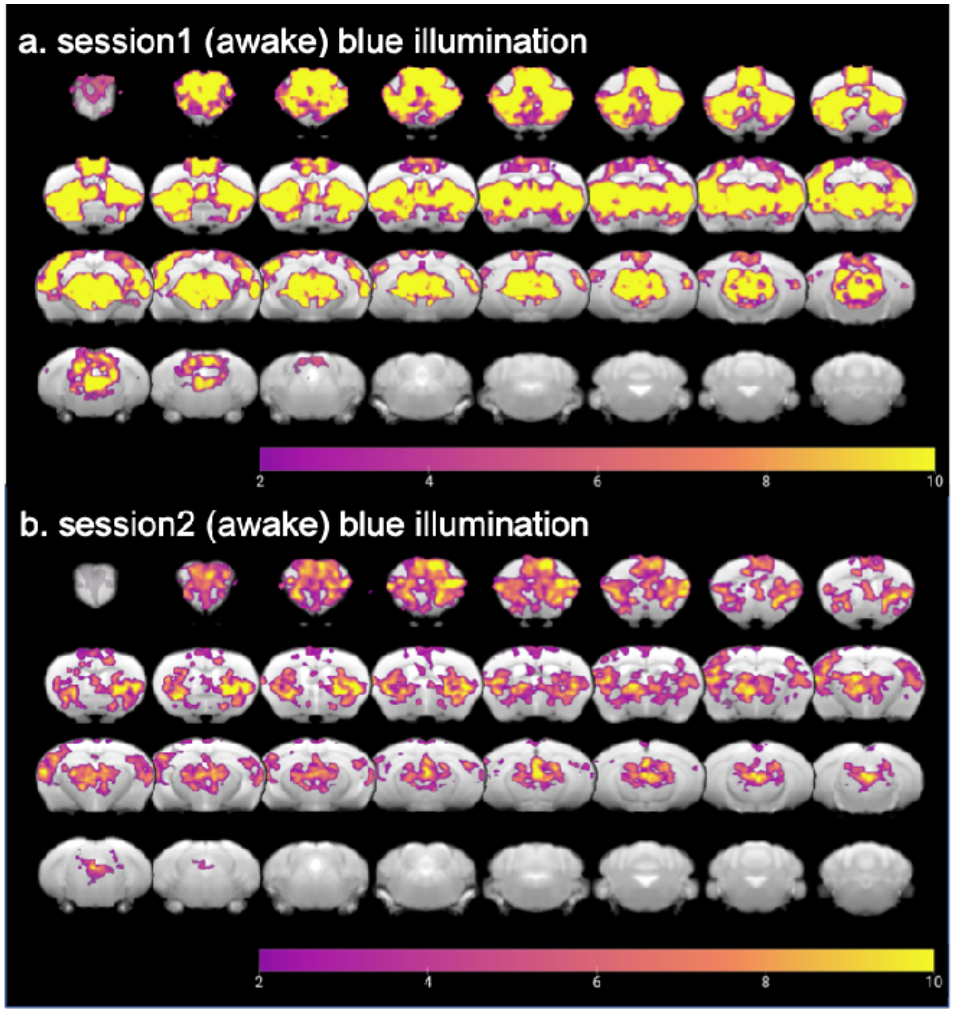

Supplementary Figure S3. (a) Functional map of transgenic mice with blue illumination in session 1 ($p < 0.05$, uncorrected, Transgenic: $n = 8$). (b) Functional map of transgenic mice with blue illumination in replication session ($p < 0.05$, uncorrected, Transgenic: $n = 7$).

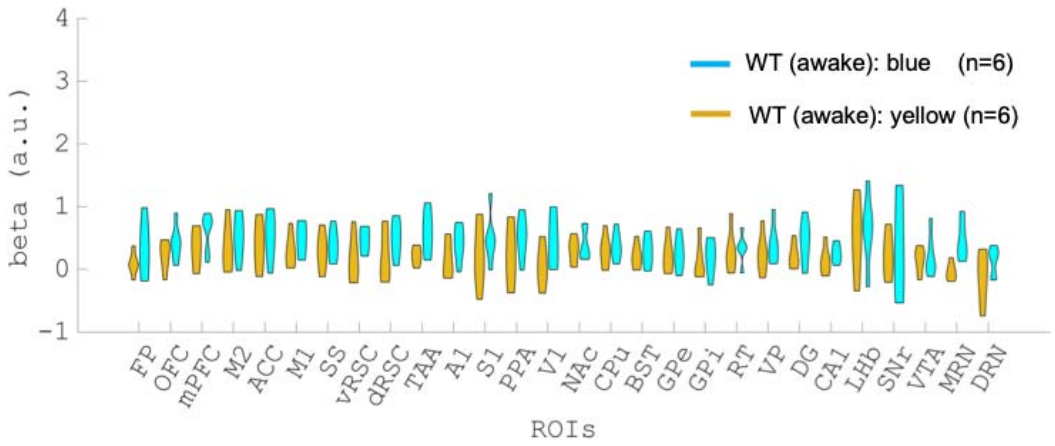

Supplementary Figure S4. Comparison of beta values in multiple ROIs with the WT group (n = 6). Beta values were obtained from GLM analysis in session 1, and were extracted and averaged based on ROIs from the Allen Brain Atlas (Table1.). The difference of beta values between blue and yellow illumination sessions were contrasted in the WT group. Cyan and yellow colors indicate blue and yellow illumination trials, respectively.

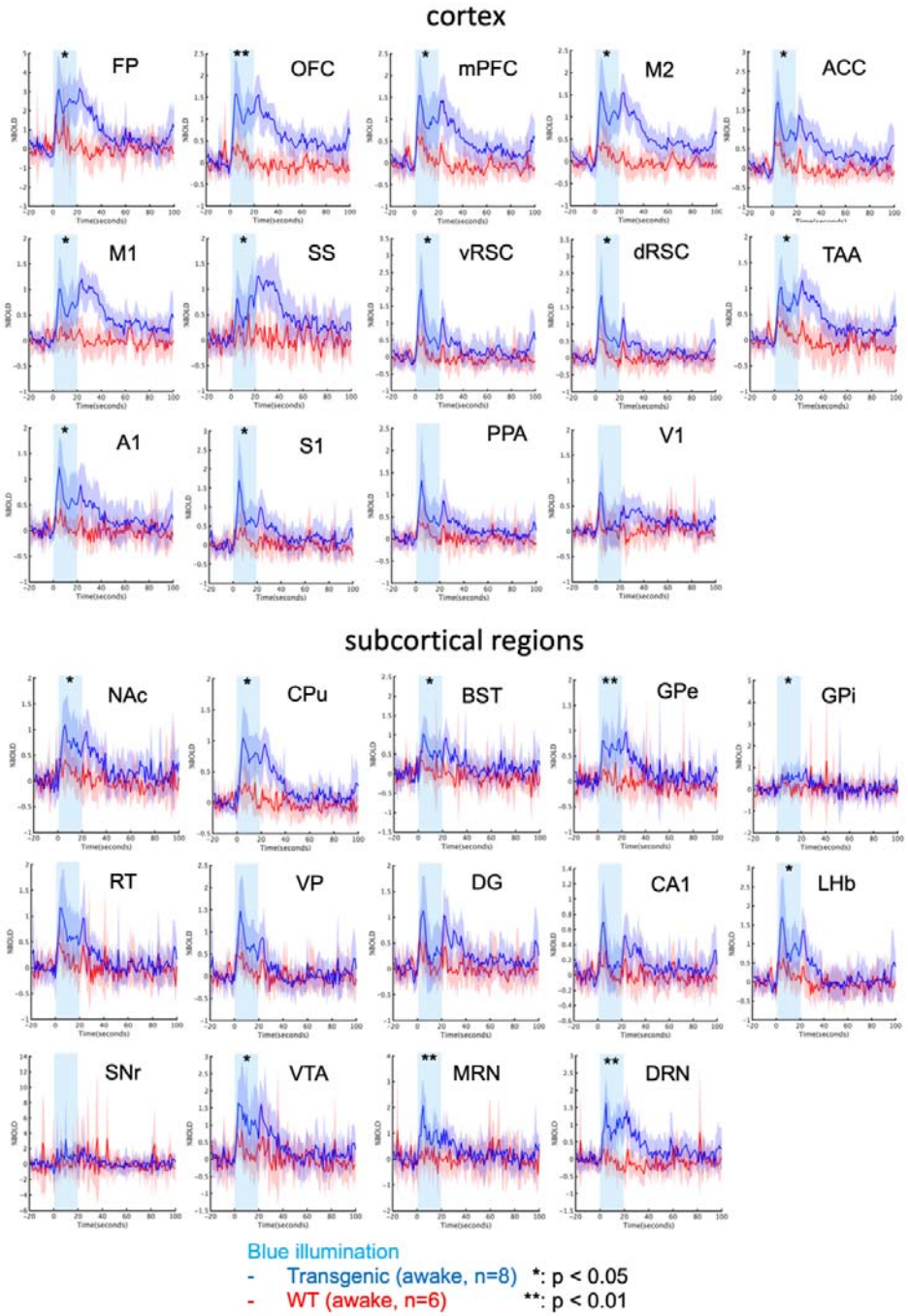

Supplementary Figure S5. Average % BOLD responses to blue illumination in the session 1. Time series of % BOLD responses to yellow illumination in each mouse were averaged at the onset of illumination. Average % BOLD responses were contrasted between the transgenic (n = 8) and WT groups (n = 6). Blue illumination (1.0 s; 473 nm) was applied at the onset of stimulation, and yellow illumination (1.0 second; 593 nm) followed the offset of stimulation 20 s after blue illumination. Cyan highlighting indicates the stimulation duration for 20 s. * and ** indicate statistical p values under 0.05 and 0.01, respectively (corrected with FDR).

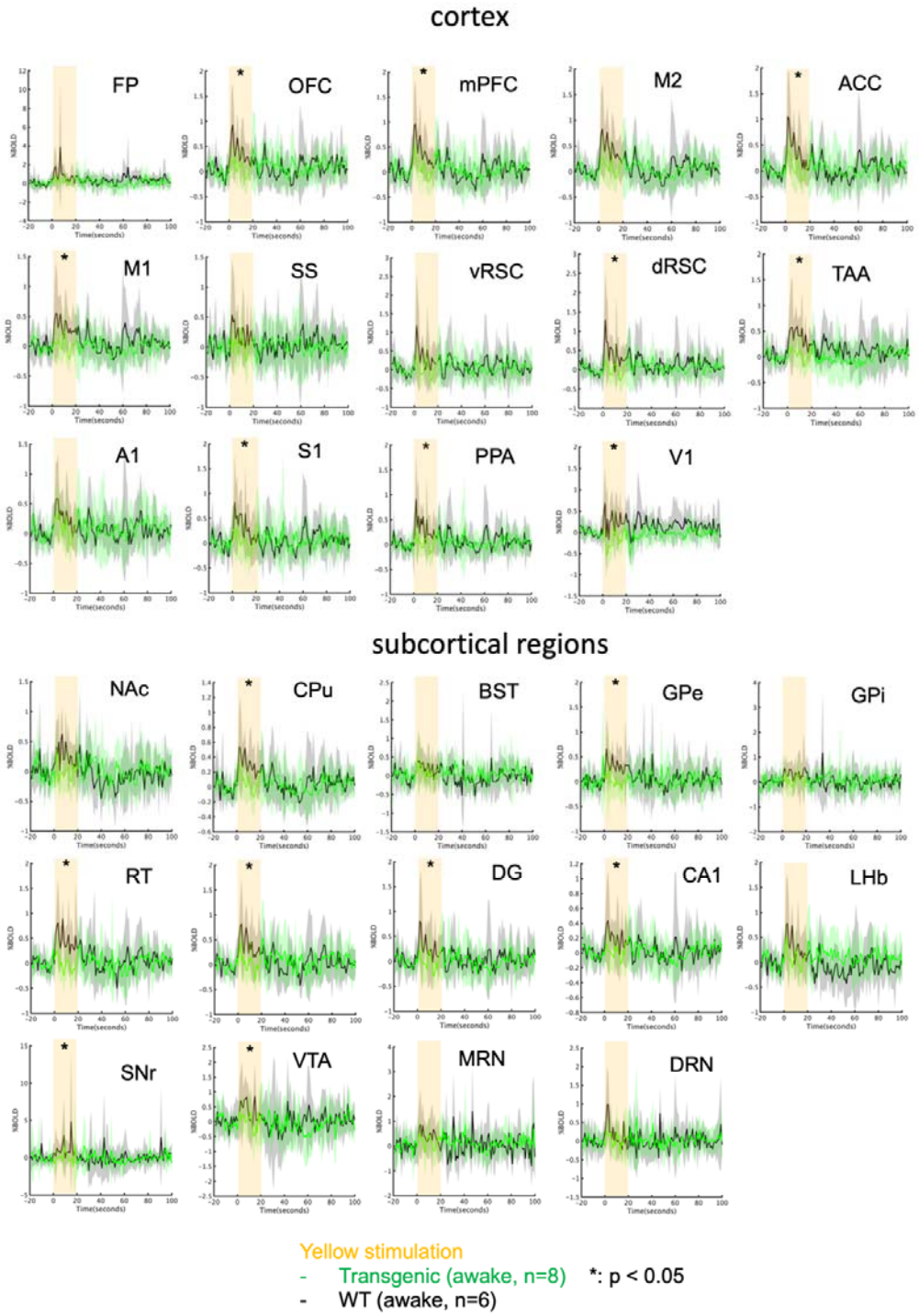

Supplementary Figure S6. Average % BOLD responses of yellow illumination in session 1. Time series of % BOLD responses to yellow illumination in each mouse were averaged at the onset of illumination. Average % BOLD responses were contrasted between the transgenic (n = 8) and WT groups (n = 6). Yellow highlighting indicates the stimulus duration for 20 s. * indicate statistical p values under 0.05 (corrected with FDR).

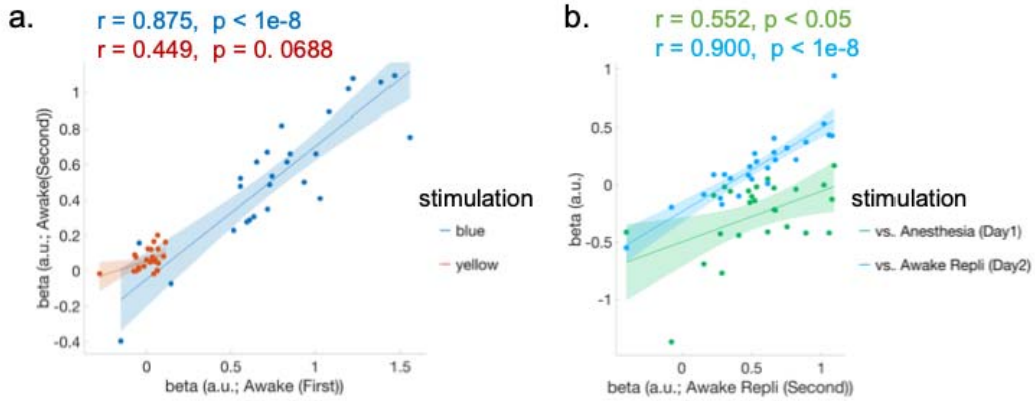

Supplementary Figure S7. (a) Replication of average beta values from GLM to blue stimulation between sessions 1 and 2 in transgenic mice. Statistically significant correlation was found in blue photo-stimulation ($r = 0.875$, $p < 1e-8$), but not in yellow photo-stimulation ($r = 0.449$, $p = 0.0688$). (b) Relationship of average regional beta values from GLM to blue photo-stimulation between session 2 and sessions 3 and 4 in transgenic mice. Statistically significant correlations were found in session 3 under general anesthetics ($r = 0.552$, $p < 0.05$) and in session 4 without general anesthesia ($r = 0.900$, $p < 1e^{-8}$).

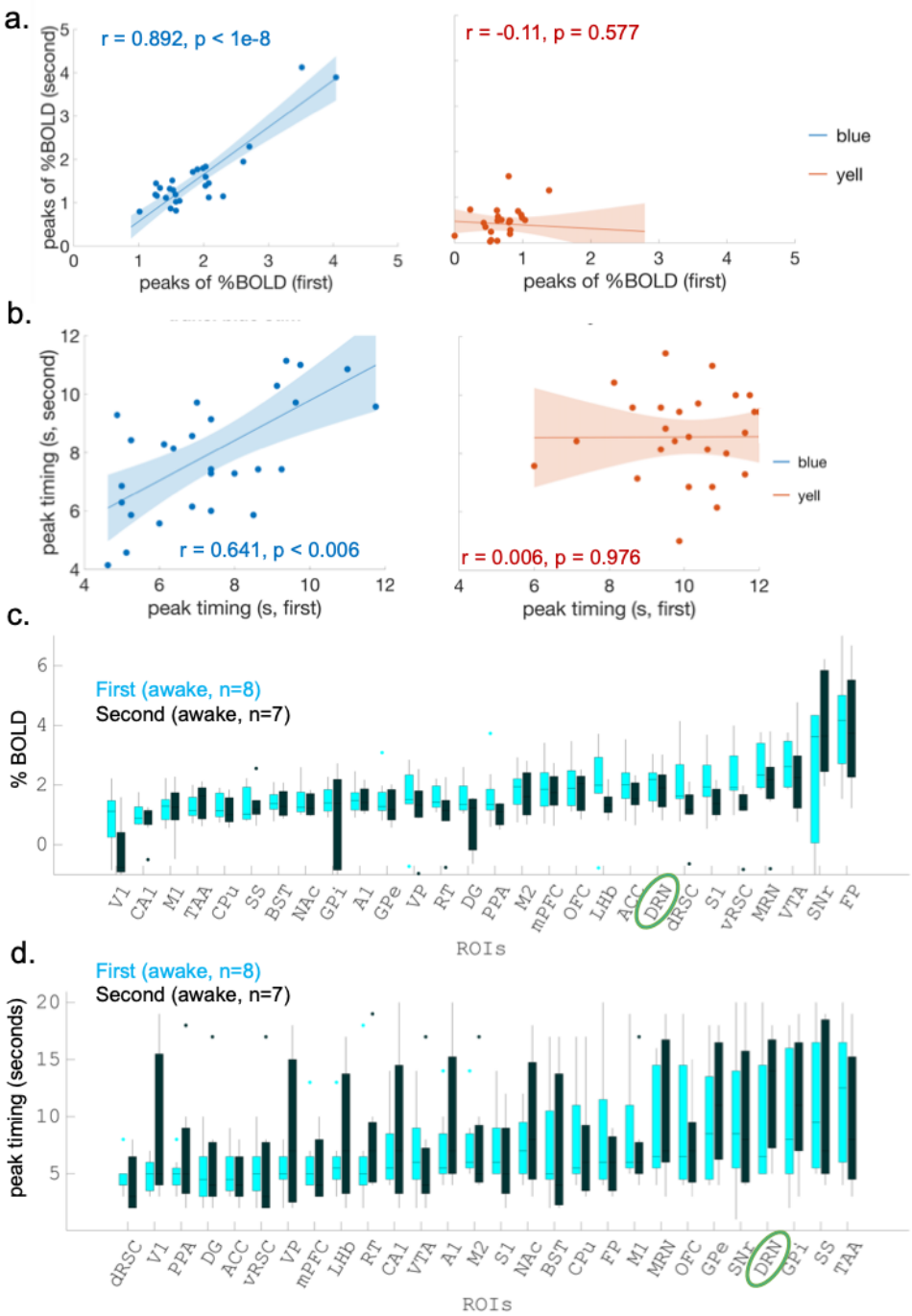

Supplementary Figure S8. (a) Replication of peaks of average % BOLD signals between sessions 1 and 2 in transgenic mice. Statistically significant correlation between peaks of % BOLD responses to blue photo-stimulation in sessions 1 and 2 was found, but not to yellow photo-stimulation (blue illumination: r = 0.8863, p < 1e-8; yellow photo stimulation: r = -0.06, p = 0.766). (b) Replication of peaks of average % BOLD signals between sessions 1 and 2 in transgenic mice. Statistically significant correlation between peak timings of % BOLD responses to blue photo-stimulation in sessions 1 and 2 was found but not to yellow photo-stimulation (blue illumination: r = 0.6785, p < 0.005; yellow photo stimulation: r = 0.0369, p = 0.8551). (c) Alignment of peaks of regional % BOLD signals in sessions 1 and 2. Peaks of % BOLD

signals are sorted in ascending order. (d) Alignment of peak timing of regional % BOLD signals in sessions 1 and 2. Peak timings of regional % BOLD signals are sorted in ascending order.

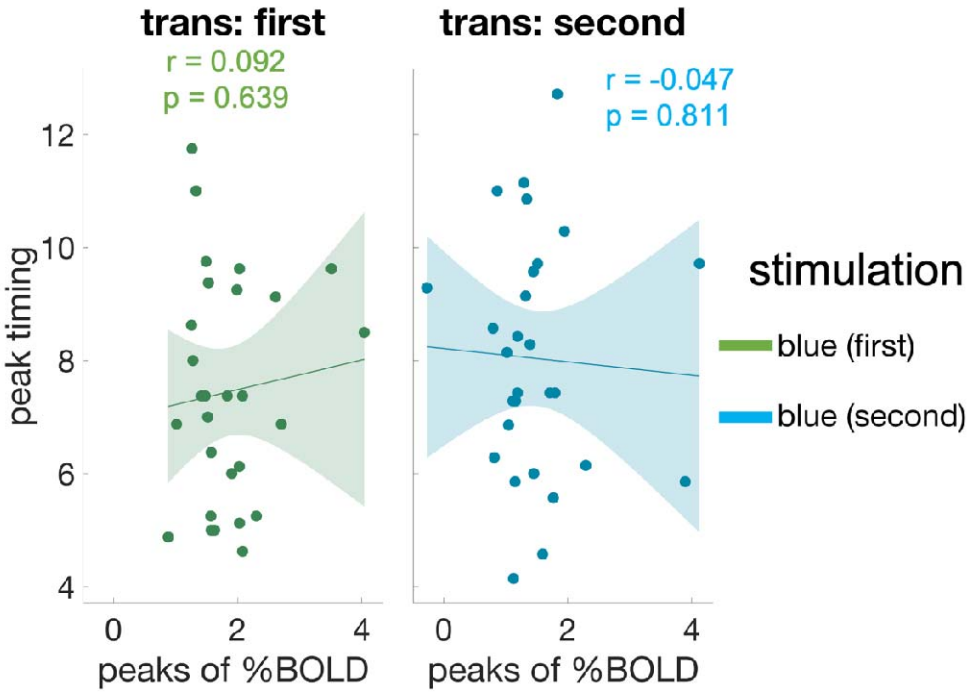

Supplementary Figure S9. Association between peak timing and peaks of average %BOLD signals in sessions 1 and 2. No statistically significant correlations between peak timing and peaks of photo-stimulated %BOLD signals were found in either session (session 1: r = 0.092, p = 0.639; session 2: r = -0.047, p = 0.811).

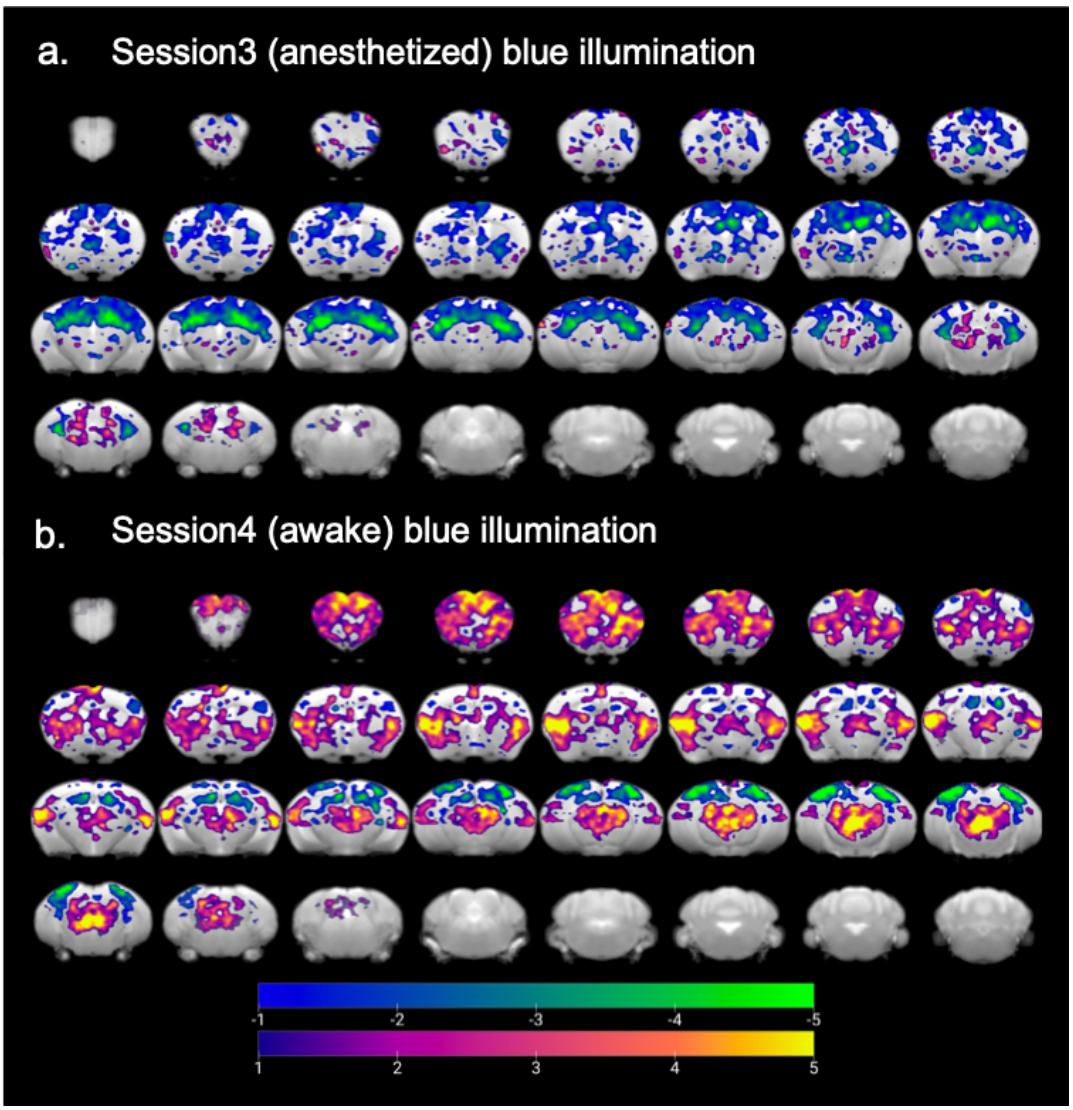

Supplementary Figure S10. (a) Functional map of transgenic mice (n = 7) with blue illumination in session 3 under anesthesia (t > 1, uncorrected). (b) Functional map of transgenic mice (n = 7) with blue illumination in session 4 without anesthesia (t > 1, uncorrected).

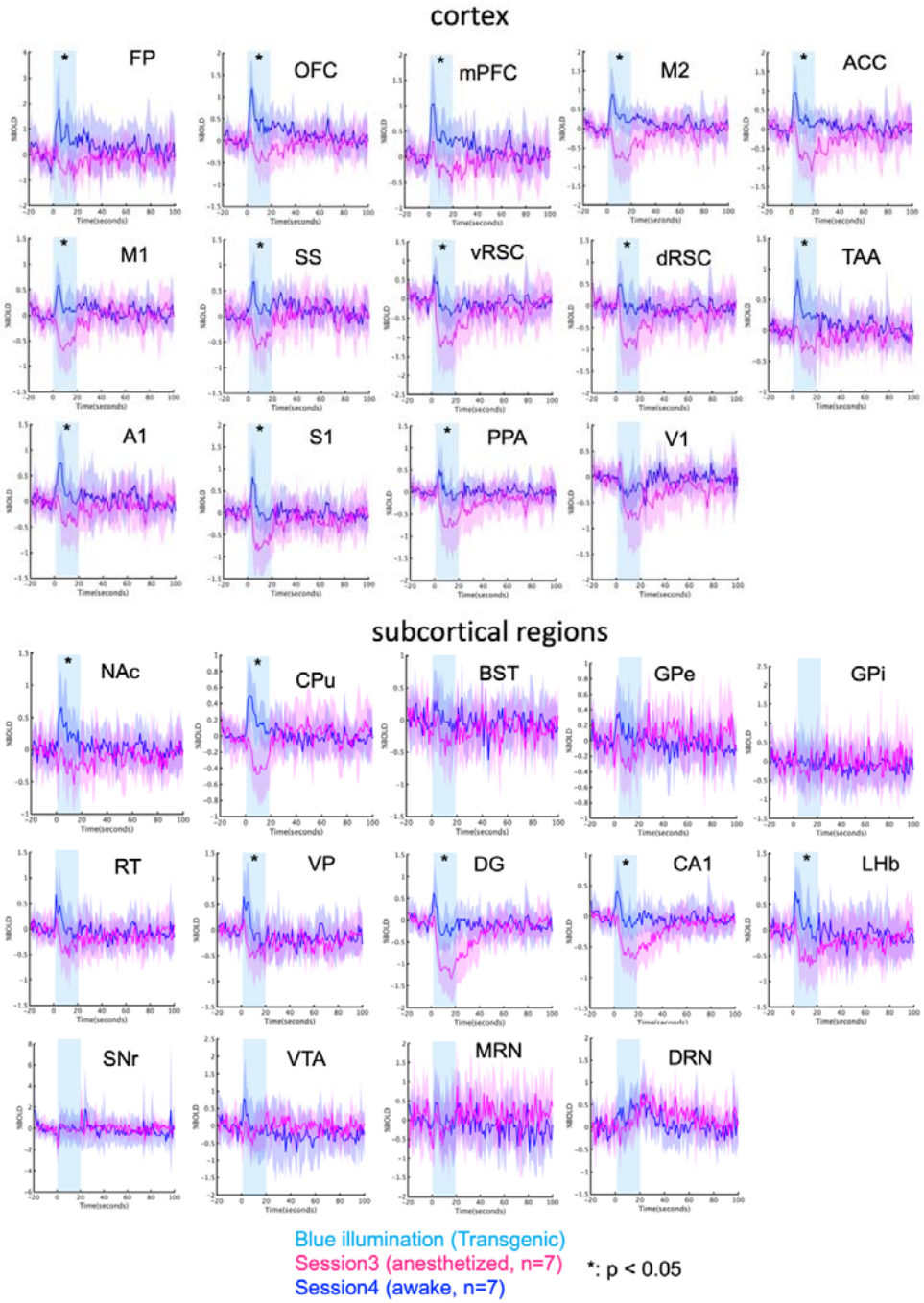

Supplementary Figure S11. Average % BOLD responses to blue illumination in sessions 3 and 4. Time series of % BOLD responses by blue illumination in each mouse were averaged at the onset of illumination. Average % BOLD responses were contrasted between sessions 3 and 4 in the transgenic group (n = 7). Blue illumination (1.0 s; 473 nm) was applied at the onset of stimulation, yellow illumination (1.0 second; 593 nm) followed the offset of stimulation 20 s after blue illumination. Cyan highlighting indicates the stimulus duration for 20 s. * indicate statistical p values under 0.05 (corrected with FDR).

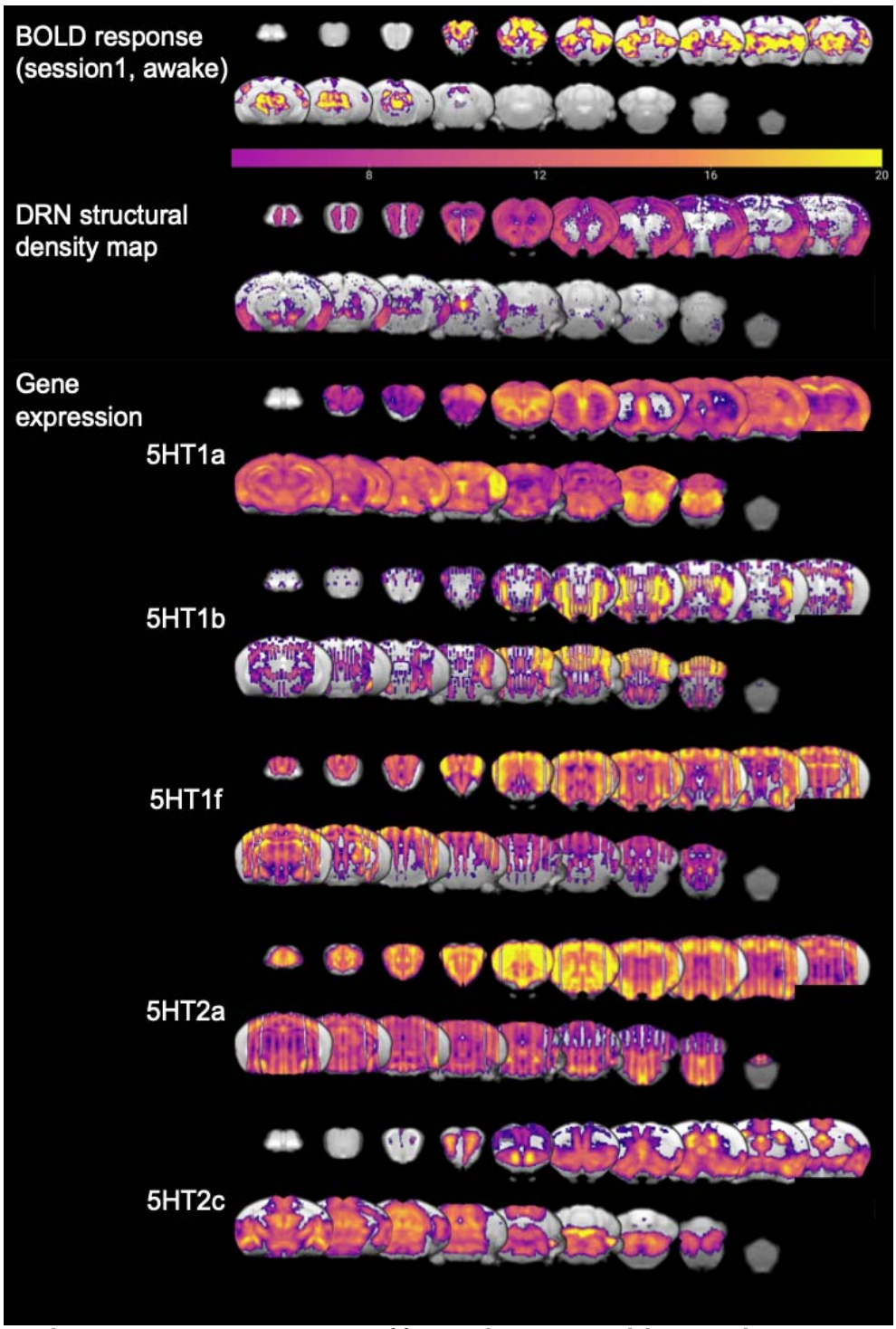

Supplementary Figure S12. Comparison of functional map, structural density, and gene expression maps. The functional map from session 1 under blue illumination was aligned with structural density and gene expression maps. The structural density map and gene expression of serotonin receptors are obtained from the mouse brain database of the Allen Brain Institute (Experimental IDs: 480074702 (5HT projection), 79556616 (5HT1a), 583 (5HT1b), 69859867 (5HT1f), 81671344 (5HT2a), and 73636098 (5HT2c)).

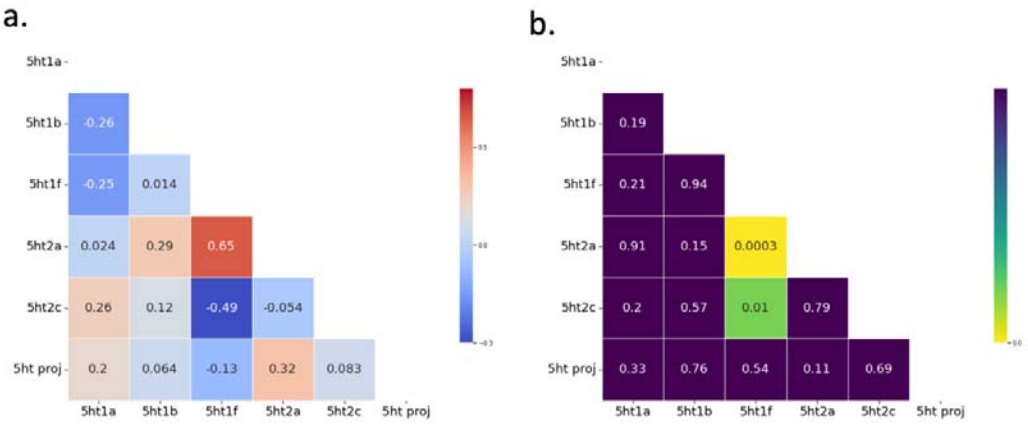

Supplementary Figure S13. Correlation between 5HT projection density and expression profiles of serotonin receptors. (a) Pearson's correlation 5HT projection density and expression profiles of serotonin receptors. (b) Corresponding statistical p values of the correlation between 5HT projection density and expression profiles of serotonin receptors ($p < 0.05$, uncorrected).

References

1. Hikishima, K., et al., In vivo microscopic voxel-based morphometry with a brain template to characterize strain-specific structures in the mouse brain. Sci Rep, 2017. 7(1): p. 85.
2. Morel, P., Gramm: grammar of graphics plotting in Matlab. Journal of Open Source Software, 2018. 3(23): p. 568.
3. Spisak, T., et al., Probabilistic TFCE: A generalized combination of cluster size and voxel intensity to increase statistical power. Neuroimage, 2019. 185: p. 12-26.